W&M ScholarWorks

Dissertations, Theses, and Masters Projects

Theses, Dissertations, & Master Projects

1981

Ultrasonic determination of thermoelastic properties of stressed solids

Engmin J. Chern

College of William & Mary - Arts & Sciences

Follow this and additional works at: https://scholarworks.wm.edu/etd

Part of the Condensed Matter Physics Commons

Recommended Citation

Chern, Engmin J., "Ultrasonic determination of thermoelastic properties of stressed solids" (1981). *Dissertations, Theses, and Masters Projects.* Paper 1539623724.
https://dx.doi.org/doi:10.21220/s2-5hpy-3c94

This Dissertation is brought to you for free and open access by the Theses, Dissertations, & Master Projects at W&M ScholarWorks. It has been accepted for inclusion in Dissertations, Theses, and Masters Projects by an authorized administrator of W&M ScholarWorks. For more information, please contact scholarworks@wm.edu.

INFORMATION TO USERS

This was produced from a copy of a document sent to us for microfilming. While the most advanced technological means to photograph and reproduce this document have been used, the quality is heavily dependent upon the quality of the material submitted.

The following explanation of techniques is provided to help you understand markings or notations which may appear on this reproduction.

1. The sign or "target" for pages apparently lacking from the document photographed is "Missing Page(s)". If it was possible to obtain the missing page(s) or section, they are spliced into the film along with adjacent pages. This may have necessitated cutting through an image and duplicating adjacent pages to assure you of complete continuity.
2. When an image on the film is obliterated with a round black mark it is an indication that the film inspector noticed either blurred copy because of movement during exposure, or duplicate copy. Unless we meant to delete copyrighted materials that should not have been filmed, you will find a good image of the page in the adjacent frame. If copyrighted materials were deleted you will find a target note listing the pages in the adjacent frame.
3. When a map, drawing or chart, etc., is part of the material being photographed the photographer has followed a definite method in "sectioning" the material. It is customary to begin filming at the upper left hand corner of a large sheet and to continue from left to right in equal sections with small overlaps. If necessary, sectioning is continued again—beginning below the first row and continuing on until complete.
4. For any illustrations that cannot be reproduced satisfactorily by xerography, photographic prints can be purchased at additional cost and tipped into your xerographic copy. Requests can be made to our Dissertations Customer Services Department.
5. Some pages in any document may have indistinct print. In all cases we have filmed the best available copy.

University
Microfilms
International

300 N. ZEEB RD., ANN ARBOR, MI 48106

8206126

CHERN, ENGMIN JAMES

ULTRASONIC DETERMINATION OF THERMOELASTIC PROPERTIES OF STRESSED SOLIDS

The College of William and Mary in Virginia PH.D. 1981

University
Microfilms
International 300 N. Zeeb Road, Ann Arbor, MI 48106

ULTRASONIC DETERMINATION OF THERMOELASTIC PROPERTIES OF STRESSED SOLIDS

A Dissertation

Presented to

The Faculty of the Department of Physics

The College of William and Mary in Virginia

In Partial Fulfillment

Of the Requirements for the Degree of

Doctor of Philosophy

By

Engmin J. Chern

1981

APPROVAL SHEET

This dissertation is submitted in partial fulfillment of
the requirements for the degree of

Doctor of Philosophy

Author

Approved, December 1981

12-11-81
J. S. Heyman, Chairman

John H. Cantrell, Jr.
J. H. Cantrell, Jr.
NASA Langley Research Center

H. E. Schone

M S Conradi
M. S. Conradi

W. J. Kossler

T. A. Zang
Department of Mathematics and Computer Science

TABLE OF CONTENTS

Page

ACKNOWLEDGMENTS v

LIST OF TABLES vi

LIST OF FIGURES vii

ABSTRACT ix

I. INTRODUCTION 2

II. THERMOELASTIC THEORY OF STRESSED SOLIDS 4

1. Small amplitude elastic wave propagation in stressed solids 4

2. Expansion of final state small amplitude wave propagation parameters in terms of initial state parameters 10

3. Stress derivatives of acoustic natural velocity (stress acoustic constants) and strain acoustic constants 18

4. Temperature dependence of acoustic natural velocity (thermal acoustic constants) and the stress derivative of thermal acoustic constants . . . 22

III. EXPERIMENTAL TECHNIQUES 27

1. Measurement considerations 27

2. Ultrasonic measurement techniques 35

IV. RESULTS AND DISCUSSION 46

1. Axial stress measurements 46

2. Thermal acoustic stress measurements 50

3. Relative slope invariance of velocity-stress and strain-stress curves 56

APPENDIX 61

Page

REFERENCES 75

ACKNOWLEDGMENTS

I would like to thank my thesis advisor, Dr. Joseph S. Heyman, for his direction and support of this research. Very special thanks are due to my co-advisor, Dr. John H. Cantrell, Jr., for his many valuable discussions of the theory and experiments.

I would also like to thank my other associates in the Instrument Research Division of NASA Langley Research Center: Dr. W. P. Winfree for his suggestions; Dr. H. I. Ringermacher, Dr. G. H. Brandenburger, Mr. H. D. Hendricks, Mr. W. E. Miller, and Dr. C. J. Magee for their comments. I am indebted to Mr. F. D. Stone, Mr. J. A. Harman, and Mr. T. C. Steele for their technical assistance. I sincerely appreciate Ms. Rise' M. Williams for typing this thesis.

I wish to express my gratitude to the faculty and staff members of the Physics Department for their support of the program, particularly to Dr. Harlan E. Schone for serving as my liaison professor, Dr. Mark S. Conradi for his suggestions, and Mrs. Sylvia J. Stout and Mrs. Thea N. Bartos for handling the voluminous paper work. It is an honor and a great experience to interact with NASA Langley Research Center.

I thank Mr. and Mrs. Glenn R. Winters and all my good friends for their constant encouragement. Finally, I thank my family, especially my parents and my wife; their sacrifices and understanding have made this possible.

LIST OF TABLES

Table Page

1. Experimental results of Salama and Ling. Compressional stress is applied in the direction perpendicular to wave propagation 54

2. Present experimental results. Tensile stress is applied along the direction of wave propagation 55

3. R values of isotopic materials calculated from elastic coefficients and from present work 59

LIST OF FIGURES

Figure Page

1. Effect of mode converted waves on the spectrum of a cylindrical resonator 29

2. Variation of acoustic intensity I with distance resulting from diffraction 31

3. The equivalent circuit of the capacitive detector and tuning circuit 34

4. Block diagram of the frequency tracking technique (tone-burst spectroscopy) for reflection configuration . . 37

5. Block diagram of the frequency tracking technique for transmission configuration 38

6. Block diagram of the pulsed phase locked loop 39

7. Block diagram of the thermal stress test system 44

8. Typical stress-acoustic, stress-strain and stress-true velocity data for an aluminum sample 47

9. Stress acoustic response for various materials 48

10. Experimental data for temperature, strain and $\Delta f/f$ as a function of time for step loading/unloading of an aluminum sample 49

11. Typical experimental data of normalized frequency change with respect to temperature 51

12. Thermal acoustic constants shown as a function of material stress 52

13. Percent error in the value of the velocity of sound, V_s as a function of δ for various correction formulas in one transducer reflection case 66

14. Percent error in V_s as a function of δ for several pairs of mechanical resonances 67

LIST OF FIGURES (Continued)

Figure Page

15. Results of computer simulated experiments comparing percent error in V_s as a function of frequency for 2.25 MHz PZT transducer bonded to an aluminum sample ($\delta = 0.109$) 69

16. Plot of percent error for various bond thickness in one transducer case 71

ABSTRACT

We present a thermoelastic derivation of ultrasonic waves propagating in a solid in which an applied homogeneous stress is superimposed on a nonzero initial stress. We also derive the temperature dependence of the elastic coefficients and the linear relationship between the applied stress and a newly defined parameter - the thermal acoustic constant. The stress acoustic constant is defined and its relationship to the acoustic natural velocity is discussed. Experimental considerations pertinent to the ultrasonic measurement techniques used in the investigation are described. The results of the stress-strain and thermal strain experiments verify the predictions of the theory. Finally, we derive an improved formula for correcting the effects of the transducer and the transducer bonding material in ultrasonic standing wave phase velocity measurements. The results are verified by computer models and laboratory experiments.

ULTRASONIC DETERMINATION OF THERMOELASTIC PROPERTIES OF STRESSED SOLIDS

INTRODUCTION

From the atomic point of view, a solid is a complicated collection of electrons and lattice particles. However, many nonlinear properties of solids such as thermal expansion, thermal conductivity, the stress dependence of elastic wave velocity and the temperature dependence of elastic velocity can be determined from constants obtained by propagating an ultrasonic wave in the sample.[1-3]

In the Debye model of solids,[4,5] the lattice vibration frequencies are approximated by long wavelength acoustic standing wave modes of a nondispersive elastic medium.[6] To provide a complete description of the nonlinear thermoelastic properties of solids, it is necessary to cast the equations describing elastic wave propagation in solids in a form explicitly involving the initial stress.[7,8] It is also necessary to use finite strain parameters instead of infinitesimal strain parameters to describe the nonlinear effects of solids. In addition, in order to characterize the adiabatic and isothermal processes, our derivations are based on a model involving thermodynamic potential energies, the internal energy and the Helmholtz free energy, rather than on a material elastic energy which is entropy and temperature independent.

It is not the purpose of this research to determine the higher order elastic constants. Rather, we wish to examine the physical properties of stressed solids from the experimentally determined stress acoustic constants and the thermal acoustic constants in accordance with recently developed ultrasonic theories[7-9] and techniques.[10,11] The stress acoustic constants are defined as the fractional change in the resonant standing wave frequency of a solid per unit applied stress[8] and is shown to be equal to the fractional change in the acoustic natural velocity in the solid. Similarly, the thermal acoustic constants are defined as the fractional change in the solid resonance frequency per unit change in temperature.[9]

In Chapter II, we present a thermoelastic description of ultrasonic waves propagating in a solid having a homogeneous stress superimposed on an initial stress. The stress acoustic constants and their relationship to acoustic natural velocity are fully discussed. We also derive the temperature dependence of elastic coefficients and the linear relationship between the applied stress and the thermal acoustic constants.

The experimental considerations and ultrasonic measurement techniques used in the present investigation are described in Chapter III. In Chapter IV, we present the experimental results which verify the predictions of the theory presented in Chapter II.

Finally, in the Appendix, we present new formulas which result in more accurate determination of acoustic velocities by correcting for transducer and bond effects for ultrasonic standing wave phase velocity measurements.

II. THERMOELASTIC THEORY OF STRESSED SOLIDS

1. Small amplitude elastic wave propagation in stressed solids.

The thermoelastic properties of stressed solids are strongly related to the behavior of the lattice particles.[12] Consider a solid which consists of N lattice particles. From Bose-Einstein statistics, the number of phonon particles in a state can be written as[13]

$$n_s = \frac{1}{\exp(\hbar\omega_s/k_B T) - 1} \tag{1}$$

where ω_s is the angular vibration frequency of s state, s represents one of the 3N states of modal vibration, k_B is Boltzmann constant and T is temperature. The internal energy of the system can be expressed in the adiabiatic approximation as[14]

$$U = \Phi_o + \sum_{s=1}^{3N} (\tfrac{1}{2} + n_s)\,\hbar\omega_s \tag{2}$$

where Φ_o is the thermodynamic potential energy of the system when the lattice particles are at rest in their mean positions. Since lattice particles move only a small amount from their equilibrium positions, we can expand the initial energy in a Taylor's series about their equilibrium positions in terms of deformation parameters. The harmonic approximation is obtained by keeping only the first nonzero (quadratic) term in the expansion. This approximation describes the linear elastic properties of solids. To describe the anharmonic properties of solids such as thermal expansion, ultrasonic harmonic generation, and thermal conductivity,[15] the quasiharmonic approximation is often used. In the quasiharmonic approximation, Φ_o and ω_s are not explicitly temperature dependent, but indirectly temperature dependent through the temperature dependence of the lattice dimensions. The temperature dependence of material parameters can be obtained explicitly from the Helmholtz free energy. The Helmholtz free energy is defined by[13]

$$F = U - TS \tag{3}$$

where S is the entropy. The Helmholtz free energy can be written as[4]

$$F = \Phi_o + k_B T \sum_{s=1}^{3N} \ln \left[2 \sinh \left(\hbar\omega_s / 2k_B T\right)\right] \tag{4}$$

The internal energy U is used to describe adiabatic processes in which the functional dependent variables are temperature T and the stresses; independent variables are entropy S and coordinate parameters $\vec{x}$. The Helmoltz free energy is used to describe isothermal processes in which the dependent variables are entropy S and the stresses; independent variables are temperature T and coordinate parameters $\vec{x}$.

To derive the elastic wave equation of the solid, we first assume the solid to be a nondispersive elastic continuum. Let the Cartesian coordinates of a material particle of the solid in the initial state be $\vec{a}$ and the Cartesian coordinates of the same particle in some stressed state at time t be $\vec{x}$. Since the internal energy U and the Helmholtz free energy F depend only on the relative position of the material particle $(\vec{x})$, it is convenient to express the functional dependence of U and F in terms of rotationally invariant Lagrangian strains η_{ij} and the initial particle positions $(\vec{a})$.

Hence, we may write

$$U(\vec{x}, S) = U(\vec{a}, \eta_{ij}, S) \tag{5}$$

It is necessary to point out that equation (5) is valid when the deformation varies significantly only over distance large compared to the range of effective interactions in the solid. For the case of elastic wave propagation, the wavelength must be large compared to the range of interactions. This is the long wavelength continuum approximation. If the wavelength is too short, dispersion occurs and the lattice dynamics theory applies.

In order to obtain the equations of adiabatic elastic wave motion, it is convenient to expand the internal energy in a power series of the Lagrangian strains defined by[16]

$$\eta_{ij} = \tfrac{1}{2} (\alpha_{ki}\ \alpha_{kj} - \delta_{ij}) \tag{6}$$

where δ_{ij} are the usual Kronecker deltas and the transformation coefficients α_{ij} are defined by

$$\alpha_{ij} = \frac{\partial x_i}{\partial a_j} \tag{7}$$

Here we have adopted the Einstein convention of summation over repeated indices. Expanding the internal energy per unit volume $\rho_1 U\ (\vec{a}, \eta_{ij}, S)$ in terms of Lagrangian strains about the initial state $(\vec{a})$, we get

$$\rho_1 U\ (\vec{a}, \eta_{ij}, S) = \rho_1 U\ (\vec{a}, o, S) + C_{ij}\ \eta_{ij} + \tfrac{1}{2} C_{ijk\ell}\ \eta_{ij}\ \eta_{k\ell} + 1/3!\ C_{ijk\ell mn}\ \eta_{ij}\ \eta_{k\ell}\ \eta_{mn} + \ldots \tag{8}$$

Where $\rho_1 = \rho(\vec{a})$ is the initial state mass density of the material. The coefficients C_{ij}, $C_{ijk\ell}$ and $C_{ijk\ell mn}$ are isentropic first, second and third order elastic constants respectively defined as

$$C_{ij} = \rho_1 \ (\partial U/\partial \eta_{ij}) \tag{9}$$

$$C_{ijk\ell} = \rho_1 \ (\partial^2 U/\partial \eta_{ij} \ \partial \eta_{k\ell}) \tag{10}$$

and

$$C_{ijk\ell mn} = \rho_1 \ (\partial^3 U/\partial \eta_{ij} \ \partial \eta_{k\ell} \ \partial \eta_{mn}) \tag{11}$$

evaluated at $(\vec{a})$. Similarly, we can expand the Helmholtz free energy per unit volume in the initial state $\rho_1 F \ (\vec{a}, \eta_{ij}, T)$ in terms of Lagrangian strains. In this case, the elastic constants are now the isothermal elastic constants instead of isentropic elastic constants. The first order strain derivative of $\rho_1 U$ and $\rho_1 F$ are the tensional stress components evaluated at the initial state configuration. Since they are evaluated at thermodynamic equilibrium, we have

$$\partial(\rho_1 U)/\partial \eta_{ij} = \partial(\rho_1 F)/\partial \eta_{ij} = \sigma_{ij} \ (\vec{a}) \tag{12}$$

For isentropic processes, the Lagrangian L can be expressed as

$$L = \tfrac{1}{2} \rho_1 \ \dot{x}_i \ \dot{x}_i - \rho_1 U \ (\vec{a}, \eta_{ij}, S) \tag{13}$$

The thermoelastic wave equation can then be obtained by substituting equation (13) into Lagrange's equation of motion

$$\frac{d}{dt} \left(\frac{\partial L}{\partial \dot{x}_i}\right) + \frac{d}{da_j} \left(\frac{\partial L}{\partial \alpha_{ij}}\right) - \frac{\partial L}{\partial x_i} = 0 \tag{14}$$

where $\dot{x}_i = \partial x_i/\partial t$, t is the time. We obtain

$$\rho_1 x_i = \frac{d}{da_j}\left[\alpha_{ik}\frac{\partial(\rho_1 U)}{\partial \eta_{jk}}\right] \tag{15}$$

Equation (15) is the general isentropic elastic wave equation valid for dissipationless solids of any symmetry. We may rewrite equation (8) as

$$\frac{\partial(\rho_1 U)}{\partial \eta_{ij}} = \sigma_{ij}(\vec{a}) + \tfrac{1}{2} C_{ijk\ell}(\alpha_{mk}\alpha_{m\ell} - \delta_{k\ell}) + \ldots \tag{16}$$

Substituting equation (16) into equation (15), we obtain the isentropic linear wave equations

$$\rho_1 \ddot{x}_i = [\sigma_{j\ell}(\vec{a})\,\delta_{ik} + C_{ijk\ell}]\frac{\partial^2 x_k}{\partial a_j \partial a_\ell} \tag{17}$$

For isothermal processes, equation (17) still holds except that the elastic constants are isothermal elastic constants.

We assume a plane solution to the linear wave equation (17) has the form

$$u_i = x_i - a_i = A_i\,|\vec{u}|\cos(k_j a_j - \omega t) \tag{18}$$

where u_i are the particle displacements, a_i are the constant material coordinates, A_i is the unit displacement vector, and $\omega = v/|\vec{k}|$ is the angular frequency. Substituting equation (18) into equation (17), we obtain the eigenvalue-eigenvector equations of elastic wave motion

$$\rho_1 v_q^2 A_i = [\sigma_{j\ell}(\vec{a})\,\delta_{ik} + C_{ijk\ell}]k_j k_\ell A_k \tag{19}$$

This equation is equivalent to the equation obtained by Thurston and Brugger.[1] We see from equation (19) that the wave velocity V_q depends on the initial state stress $\sigma_{j\ell}(\vec{a})$ as well as the second order elastic constants. The subscript q represents the propagating direction for which there are three independent eigenvalues representing one quasi-longitudinal and two quasi-transverse polarization directions of elastic wave propagation. For certain propagation directions of high crystalline symmetry, the three normal modes become one pure longitudinal and two pure transverse modes.

2. Expansion of final state small amplitude wave propagation parameters in terms of initial state parameters.

Consider now in addition to the initial thermodynamic stress $\sigma_{j\ell}(\vec{a})$, there is an externally applied homogeneous static stress on the solids. We shall use the perturbation approach of Cantrell[3] and Wallace[2] to obtain the equation of motion and pertinent measurement parameters for such a situation which brings the solid to a final homogeneous stress state $(\vec{\bar{a}})$. The Cartesian coordinates of a material particle in the solid which was at $\vec{a}$ in the initial state now is at the coordinates $\vec{\bar{a}}$ in the final state. We define the transformation coefficients with respect to the final state to be

$$\bar{\alpha}_{ij} = \frac{\partial x_i}{\partial \bar{a}_j} \tag{20}$$

and the Lagrangian strain parameters with respect to final the state to be

$$\bar{\eta}_{ij} = \tfrac{1}{2}\,(\bar{\alpha}_{ki}\,\bar{\alpha}_{kj} - \delta_{ij}) \tag{21}$$

Thus, the internal energy in the final stress state can be expanded in terms of Lagrangian strain parameters η_{ij} with respect to the final state as

$$\begin{aligned}\rho_2 U\,(\vec{\bar{a}},\, \bar{\eta}_{ij},\, S) &= \rho_2 U\,(\vec{\bar{a}},\, o,\, S) + \sigma_{ij}\,(\vec{\bar{a}})\,\bar{\eta}_{ij} + \\ &\tfrac{1}{2}\,\bar{C}_{ijk\ell}\,\bar{\eta}_{ij}\,\bar{\eta}_{k\ell} + 1/3!\;\bar{C}_{ijk\ell mn}\,\bar{\eta}_{ij}\,\bar{\eta}_{k\ell}\,\bar{\eta}_{mn} + \dots\end{aligned} \tag{22}$$

where $\rho_2 = \rho\,(\vec{\bar{a}})$ is the mass density of the solid in the final state and the elastic constants are defined with respect to the final state.

Similarly, we can expand the Helmholtz free energy in terms of Langrangian strain parameters with respect to the final state as in equation (22) with F in place of U. Following the same procedure as in section 1, we can obtain the eigenvalue-eigenvector equations of motion with respect to the final state as

$$\rho_2 \bar{V}_q^2 \bar{A}_i = [\, \sigma_{j\ell} (\vec{\bar{a}})\, \delta_{ik} + \bar{C}_{ijk\ell} \,]\; \bar{k}_j\, \bar{k}_\ell\, \bar{A}_k \tag{23}$$

where the bar denotes that the quantities are evaluated with respect to the final state. However, we wish to express the wave equation (23) in terms of initial state parameters. We define the transformation coefficient α'_{ij} from the initial state $\vec{a}$ to the final state $\vec{\bar{a}}$ as

$$\alpha'_{ij} = \frac{\partial \bar{a}_i}{\partial a_j} \tag{24}$$

The Lagrangian strains from the initial state to the final state is defined as

$$\eta'_{ij} = \tfrac{1}{2} (\alpha'_{ki}\, \alpha'_{kj} - \delta_{ij}) \tag{25}$$

A plane wave propagating in the direction $\vec{\bar{k}}$ in the homogeneous deformed final state and in the initial state must satisfy the phase condition

$$\bar{k}_i\, \bar{a}_i = \bar{k}_i \frac{\partial \bar{a}_i}{\partial a_j}\, a_j = \mu\, k_j\, a_j \tag{26}$$

where $\bar{k}_i\, \bar{k}_i = k_j\, k_j = 1$, and the normalization constant μ is defined such that

$$\mu^2 k_i k_i = \alpha'_{ki} \alpha'_{\ell i} \bar{k}_k \bar{k}_\ell \tag{27}$$

For homogeneous initial and applied stresses the waves remain parallel to the sample surface at which waves are launched, irrespective of the state of homogeneous stress. For this case, $\vec{k}_i \cdot \vec{a}_i = \ell_1$ which can be interpreted as the sample length of the solid in the initial state. Similarly, $\vec{\bar{k}}_i \cdot \vec{\bar{a}}_i = \ell_2$, is the sample length of the solid in the final state. The normalization constant μ in equation (27) is then obtained as

$$\mu = \frac{\bar{k}_i \bar{a}_i}{k_i a_i} = \frac{\ell_2}{\ell_1} \tag{28}$$

If we define the inverse transformation tensor β'_{ij} such that

$$\beta'_{ij} \alpha'_{jk} = \alpha'_{ij} \beta'_{jk} = \delta_{ik} \tag{29}$$

We can write the wave vectors in final state as

$$\bar{k}_i = \mu \beta'_{ji} k_j \tag{30}$$

and the Lagrangian strains defined with respect to the final state as

$$\bar{\eta}_{ij} = \tfrac{1}{2} \left(\frac{\partial x_k}{\partial \bar{a}_i} \frac{\partial x_k}{\partial \bar{a}_j} - \delta_{ij}\right) = \eta_{k\ell} \beta'_{ik} \beta'_{j\ell} \tag{31}$$

Using equations (30) and (31), the second order elastic constants defined with respect to the final state can be expressed in terms of the elastic constants with respect to the initial state as

$$\bar{C}_{ijk\ell} = \rho_2 \left(\frac{\partial^2 U}{\partial \bar{\eta}_{ij} \partial \bar{\eta}_{k\ell}}\right) = \left(\frac{\rho_2}{\rho_1}\right) \alpha'_{im} \alpha_{jn} \alpha'_{kp} \alpha'_{\ell q}$$

$$[C_{mnpq} + C_{mnpqrs} \eta'_{rs} + \ldots] \tag{32}$$

Similarly, the final state stress $\sigma_{ij}(\vec{\bar{a}})$ can be expressed in terms of the initial state stress $\sigma_{ij}(\vec{a})$ and the elastic constants defined with respect to the initial state as

$$\sigma_{ij}(\vec{\bar{a}}) = \rho_2 \left(\frac{\partial U}{\partial \bar{\eta}_{ij}}\right) = \left(\frac{\rho_2}{\rho_1}\right) \alpha'_{ik} \alpha'_{j\ell} [\sigma_{k\ell}(\vec{a}) + C_{k\ell mn} \eta'_{mn} + \ldots] \tag{33}$$

Substituting equations (31), (32), and (33) into equation (23), we obtain the equations for elastic wave velocity in the final state of the solid in terms of initial state parameters as

$$\rho_2 \bar{v}_q^2 \bar{A}_i = \mu^2 \left(\frac{\rho_2}{\rho_1}\right) \{\alpha'_{jm} \alpha'_{\ell n} [\sigma_{mn}(\vec{a}) + C_{mnpq} \eta'_{pq} + \ldots] \delta_{ik} + \alpha'_{im} \alpha'_{jn} \alpha'_{kp} \alpha'_{\ell q} [C_{mnpq} + C_{mnpqrs} \eta'_{rs} + \ldots]\} \beta'_{rj} \beta'_{s\ell} k_r k_s \bar{A}_k \tag{34}$$

The physical measurements of the wave velocity of equation (34) depend on changes in sample length in the direction of wave propagation as well as changes in density at different final states. We can eliminate the length effect by introducing the natural velocity $\bar{W}_q$ defined by Thruston and Brugger[1] as

$$\bar{W}_q = \frac{\ell_1}{\ell_2} \bar{v}_q \tag{35}$$

The natural velocity $\bar{W}_q$ is a physically measurable quantity which as we shall show in section 4 is directly proportional to the resonance frequency of the solid. Using equation (35), we can rewrite equation (34) as

$$\rho_1 \bar{W}_q^2 = \{ [\sigma_{j\ell} (\vec{a}) \delta_{ik} + C_{ijk\ell}] k_j k_\ell + [(C_{mnpq} k_m k_n \eta'_{pq} \delta_{ik}) + C_{inpq} \eta'_{kp} + C_{mnkq} \eta'_{im} + C_{inkqrs} \eta'_{rs}) k_n k_q] \} \bar{A}_i \bar{A}_k \qquad (36)$$

where we have used the expansion of α'_{ij} in terms of η'_{ij} in the equation

$$\alpha'_{ij} = \delta_{ij} + \eta'_{ij} - \tfrac{1}{2} \eta'_{ki} \eta'_{kj} + \ldots \qquad (37)$$

If we let $\bar{A}_i \bar{A}_k = A_i A_k$, we can approximate the elastic wave equation (36) to first order in the strain as

$$\rho_1 \bar{W}_q = \rho_1 W_q^2 + [2 \rho_1 W_q^2 A_m A_n + (C_{ijkl\ell mn} A_i A_k - 2\sigma_{j\ell} (\vec{a}) A_m A_n) k_j k_\ell] \eta'_{mn} \qquad (38)$$

where we have used equation (19). Equation (38) is the first order correction to the natural velocity in terms of initial state parameters. For the case where $\sigma_{j\ell} (\vec{a}) = 0$, equation (38) may be written in terms of the applied stress $\sigma_{ij} (\vec{a}') = \sigma_{ij} (\vec{\bar{a}}) - \sigma_{ij} (\vec{a})$ by using the compliance tensor $S_{ijk\ell}$ defined such that

$$S_{ijk\ell} C_{k\ell mn} = C_{ijk\ell} S_{k\ell mn} = \tfrac{1}{2} (\delta_{im} \delta_{jn} + \delta_{in} \delta_{jm}) \qquad (39)$$

and writing

$$\eta'_{ij} = S_{ijk\ell} \sigma_{k\ell} (\vec{a}') + \ldots . \qquad (40)$$

Substituting equation (40) into equation (38) and using equation (39), we obtain

$$\rho_1 \bar{W}_q^2 = \rho_1 W_q^2 + [2 \rho_1 W_q^2 A_m A_n + (C_{j\ell mn} + C_{ijk\ell mn} A_i A_k) k_j k_\ell] S_{mnrs} \sigma_{rs} (\vec{a}') \tag{41}$$

Equations (38) and (41) are general expressions for the natural velocity $\bar{W}_q$ of a solid subjected to a superimposed stress $\sigma_{ij}(\vec{a}')$ or strain η'_{ij}. The importance of the equations is that the natural velocity is written in terms of parameters defined with respect to the initial state parameters. $\sigma_{rs}(\vec{a}')$ and η'_{mn} are defined to be positive for tensile load and negative for compressional load.

For the case of isotropic solids, we obtain the acoustic natural velocity of the unstressed state from equation (19) as

$$\begin{aligned} \rho_o W_L^2 &= C_{11} \\ \rho_o W_S^2 &= C_{44} \end{aligned} \tag{42}$$

Where L denotes longitudinal wave propagation and S denotes shear wave propagation. In equation (42), we have used Voight contraction of the indices for the elastic constants.[17] From the invariance under symmetry operations, the relations of the second order elastic constants for the isotropic solids are found to be[1]

$$\begin{aligned} &C_{11} = C_{22} = C_{33} = \lambda + 2\mu \\ &C_{12} = C_{13} = C_{23} = \lambda \\ &C_{44} = C_{55} = C_{66} = \mu \\ &\text{All other } C_{ij} = 0 \end{aligned} \tag{43}$$

Where λ and μ are Lame' second order constants. Other moduli used to describe the properties of isotropic solids such as Young's modulus

E, Poisson's ratio ν, shear modulus G, and bulk modulus K can be written in terms of Lame' constants as

$$E = \mu\,(3\lambda + 2\mu)/(\lambda + \mu)$$

$$\nu = \lambda/2\,(\lambda + \mu)$$

$$G = \mu$$

$$K = \lambda + 2/3\mu \tag{44}$$

For the case of longitudinal wave propagation in an isotropic solid along the direction of applied uniaxial stress, we can express the natural velocity as

$$\rho_o\,W_L^2 = (2\mu + \lambda) + \left(\frac{\sigma}{3\lambda + 2\mu}\right)\left[\lambda + 2\ell + \frac{\lambda+\mu}{\mu}\,(2\lambda + 6\mu + 4m)\right] \tag{45}$$

where ℓ, m (and n) are Murnaghan's third order elastic constants. Hughes and Kelly[18] have derived similar equations for the true velocity in a solid (rather than natural velocity) for different propagation directions, propagation modes and applied stress directions. The relations between Murnaghan's third order elastic constants and Brugger's third order elastic constants for isotropic solids are[19]

$$C_{123} = 2\ell - 2m + n$$

$$C_{456} = \tfrac{1}{4}\,n$$

$$C_{144} = C_{255} = C_{366} = 2\ell + 4m$$

$$C_{111} = C_{222} = C_{333} = 2\ell + 4m$$

$$C_{112} = C_{223} = C_{133} = C_{113} = C_{122} = C_{233} = 2\ell$$

$$C_{155} = C_{244} = C_{344} = C_{166} = C_{266} = C_{355} = m$$

$$\text{All other } C_{ijk} = 0 \tag{46}$$

We will use equation (45) in the next section to express a newly defined measurement parameter (the stress acoustic constant)[20] in terms of elastic coefficients.

3. Stress derivatives of acoustic natural velocity (stress acoustic constants) and strain acoustic constants

We now consider an isolated one-dimensional stressed solid resonator. The propagating wave model[21,22] predicts that the mechanical resonance frequency f_m $(m = 1, 2 \ldots .)$ occurs at

$$f_m = \frac{m\vec{V}_q}{2\ell_2} \tag{47}$$

where V_q is the true wave velocity in the final state and ℓ_2 is the sample length in the final state. We note that the changes in mechanical resonance frequencies result from changes in the true wave velocity as well as changes in sample length at each stress level. The acoustic natural velocity $\bar{W}_q$ was defined by equation (35). Substituting $\bar{W}_q$ into equation (47), we obtain

$$f_m = \frac{m\bar{W}_q}{2\ell_1} \tag{48}$$

Since m is an integer and ℓ_1 is the sample length in the unstressed state, the change in resonance frequency f_m now depends only on the change in acoustic natural velocity for different stress levels. Differentiating equations (47) and (48), we obtain the fractional change in mechanical resonance frequency and acoustic natural velocity in terms of relative changes in true wave velocity and strain as

$$\frac{df_m}{f_m} = \frac{dV_q}{V_q} - \frac{d\ell}{\ell_1} = \frac{d\bar{W}_q}{W_q} \tag{49}$$

We define the stress acoustic constants H_{rs} to be the fractional change in resonance frequency per unit change in applied stress and obtain from equation (48)

$$H_{rs} = \frac{1}{f_m}\frac{\partial f_m}{\partial \sigma_{rs}} = \frac{1}{W_q}\frac{\partial \bar{W}_q}{\partial \sigma_{rs}} \tag{50}$$

We can write the stress acoustic constants in terms of elastic constants as

$$H_{rs} = \frac{1}{W_q}\frac{\partial \bar{W}_q}{\partial \sigma_{rs}} = \frac{1}{2\rho_1 W_q^2}\frac{\partial (\rho_1 \bar{W}_q^2}{\partial \sigma_{rs}} \quad \frac{1}{2\rho_1 W_q^2}[2\rho_1 W_q^2 A_m A_n +$$

$$(C_{j\ell mn} + C_{ijk\ell mn} A_i A_k - 2\sigma_{j\ell}(\vec{a}) A_m A_n) k_j k_\ell] S_{mnrs} \tag{51}$$

where the last equality follows from equation (38). We note that equation (51) is evaluated with respect to the initial state. For zero initial stress, i.e. $\sigma_{j\ell}(\vec{a}) = 0$, all the parameters are zero state parameters. For the case of isotropic solids the stress acoustic constant for the case of longitudinal wave propagation along the direction of applied tensile stress is calculated from equation (45) to be

$$H_{11} = [\lambda + 2\ell + \frac{\lambda + \mu}{\mu}(2\lambda + 6\mu + 4m)] / [2(\lambda + 2\mu)(3\lambda + 2\mu)]$$

$$= [(C_{11} - C_{12})(C_{11} + 2C_{12}) + (C_{11} + C_{12})(2C_{11} + C_{111}) - C_{12}$$

$$C_{112})] / [2C_{11}(C_{11} - C_{12})(C_{11} + 2C_{12})] \tag{52}$$

We define the strain acoustic constants R_{mn} to be the fractional change in resonance frequency per unit change in strain. Hence,

$$R_{mn} = \frac{1}{f_m}\frac{\partial f_m}{\partial \eta_{mn}} = \frac{1}{W_q}\frac{\partial \bar{W}_q}{\partial \eta_{mn}} = \frac{1}{2\rho_1 W_q^2}[2\rho_1 W_q^2 A_m A_n + (C_{j\ell mn}$$

$$+ C_{jk\ell mn} A_i A_k - 2\sigma_{j\ell} (\vec{a}) A_m A_n) k_j k_\ell] \qquad (53)$$

where the last equality follows from equation (38). From equations (50) and (53), we obtain the relationship between the stress acoustic constants H_{rs} and the strain acoustic constants R_{mn} to be

$$H_{rs} = R_{mn} S_{mnrs} \qquad (54)$$

where S_{mnrs} is the compliance coefficients defined by equation (39). Substituting S_{1111} (= S_{11} in Voigt notation) into equation (52), we obtain the expression for strain acoustic constant for the case of longitudinal wave propagating in an isotropic solid along the direction of applied tensile strain as

$$R_{11} = [(C_{11} - C_{12}) (C_{11} + 2 C_{12}) + (C_{11} + C_{12}) (2 C_{11} + C_{111}) - 2 C_{11} C_{112})] / [2 C_{11} (C_{11} + C_{12})] \qquad (55)$$

We must point out that the stress and strain acoustic constants can be obtained experimentally by simply evaluating the ratio of the change in normalized mechanical resonance frequency and the change in applied stress or strain, respectively.

It is of interest to note that the strain generalized Grüneisen parameters are defined[23] as the fractional changes in the modal phonon vibration frequencies per unit change in strain

$$\gamma^s_{ij} = - [1/\omega_s (\partial\omega_s/\partial\eta_{ij})_T]_{\eta=0} \qquad (56)$$

If we identify the long - wavelength modal phonon vibration frequencies with the coherent acoustic resonance frequencies, we obtain the relationship between the strain generalized Grüneisen parameter and strain acoustic constants to be

$$R_{mn} = -\gamma^{s}_{mn} \tag{57}$$

Hence, measurements of the strain acoustic constants are tantamount to measuring the strain generalized Grüneisen parameters. The thermodynamic Grüneisen parameter is defined by[24]

$$\gamma = \beta B_T/\rho_o C_v \tag{58}$$

where β is the volume thermal expansion coefficients, C_v is the specific heat and B_T is the isothermal bulk modulus. The relationship between the thermodynamic Grüneisen parameter and the strain generalized Grüneisen parameters in the Debye model is given elsewhere.[6] Hence, the strain acoustic constants are seen to be fundamentally related to the equation of state of Debye solids.

4. Temperature dependence of acoustic natural velocity (thermal acoustic constants) and the stress derivative of thermal acoustic constants.

The conjugation of thermoelastic and statistical mechanical theories of materials have shown that the temperature dependence of material parameters can be obtained from expansions of the Helmholtz free energy (equation (4)) in terms of lattice vibrational modes.[25,26] If we adopt the long wavelength continuum approximation and identify the material particle (actually phonon) vibrational frequencies with the coherent acoustic resonance frequencies, the temperature derivative of isothermal second order elastic constants $C^T_{ijk\ell}$ in the high temperature limit can be written as

$$(\partial C^T_{ijk\ell}/\partial T)_\eta = -\rho_o k_B \sum_{s=1}^{3N} \left(\frac{\partial \gamma^s_{ij}}{\partial \eta_{k\ell}}\right)_T \tag{59}$$

where γ^s_{ij} are strain generalized Grüneisen parameters defined by equation (56). Similarly, we can write the temperature derivative of the isothermal third order elastic constants $C^{TT}_{ijk\ell m}$ in the high temperature limit as

$$(\partial C^{TT}_{ijk\ell mn}/\partial T)_\eta = -\rho_o k_B \sum_{s=1}^{3N} \left(\frac{\partial^2 \gamma^s_{ij}}{\partial \eta_{k\ell} \partial \eta_{mn}}\right)_T \tag{60}$$

where the superscript TT represents continuous derivations of isothermal strains. If we express γ^s_{ij} in terms of elastic constants via the theory of Thurston and Brugger[1] and substitute the expression into equations (59) and (60), we obtain the temperature derivative of isothermal second and third order elastic constants in terms of the mixed isothermal - isentropic initial state elastic constants. The relationship between isentropic and isothermal second order elastic constants are given by[7]

$$C^{s}_{ijk\ell} - C^{T}_{ijk\ell} = (T/\rho_o C_v)\ \tau_{ij}\ \tau_{k\ell} \tag{61}$$

where τ_{ij} is the thermal stress tensor defined by[7]

$$\tau_{ij} = (\partial\sigma_{ij}/\partial T)_{\eta_{ij}} \quad . \tag{62}$$

For isotropic solids the relationship between isentropic and isothermal second order elastic constant C_{11} is also given by[26]

$$C^{s}_{11} - C^{T}_{11} = T\gamma^2\ \rho_o\ C_v \tag{63}$$

where the thermodynamic Grüneisen parameter γ is defined by equation (58). For a typical solid such as aluminum, $\rho_o = 2.8$ g/cm^3, $C_v = 9.0 \times 10^6$ erg/g.^{o}k, and $\gamma^2 = 4$ at room temperature ($T = 300^oK$), and the difference between isentropic and isothermal constants is calculated from equation (63) to be less than 3%. Hence, we can approximate the temperature derivative of the C_{11} elastic constant from equation (59). For example[27]

$$\partial C_{11}/\partial T = \frac{-\rho_o k_B}{2}\left[\left(\frac{3C_{11} + C_{111}}{C_{11}}\right)^2 - \left(\frac{5\ C_{111} + C_{1111}}{C_{11}}\right)\right] \quad . \tag{64}$$

We now define the thermal acoustic constants K_q for any state of stress $\sigma_{k\ell}$ to be the fractional change in acoustic natural velocity W_q per unit change in temperature and write

$$[\,K_q\,]_{\sigma_{k\ell}} = \left[\frac{1}{W_q}\left(\frac{\partial W_q}{\partial T}\right)\right]_{\sigma_{k\ell}} = \left[\frac{1}{2\rho_o W_q^2}\left(\frac{\partial \rho_o W_q^2}{\partial T}\right)\right]_{\sigma_{k\ell}} \tag{65}$$

where the derivation is evaluated at the initial temperature T_o. From equation (41), we can write the thermal acoustic constants for a state of applied stress σ_{rs} in terms of elastic constants and temperature derivatives of elastic constants as

$$[K_q]_{\sigma_{rs}} = \frac{1}{2\rho_o W_q^2} \{ \frac{\partial C_{ijk\ell}}{\partial T} k_j k_\ell A_i A_k + [2\rho_o W_q^2 A_m A_n + (C_{j\ell mn} + C_{ijk\ell mn} A_i A_k) k_j k_\ell] \beta_{mn} + [2 \frac{\partial C_{ijk\ell}}{\partial T} k_j k_\ell A_i A_k A_m A_n + (\frac{\partial C_{j\ell mn}}{\partial T} + \frac{\partial C_{ijk\ell mn}}{\partial T} A_i A_k) k_j k_\ell] \eta'_{mn} \}_{\sigma_{rs}} \tag{66}$$

where we have assumed that initial state stress is zero, i.e., $\sigma_{j\ell}(\vec{a}) = 0$, $\rho_o W_q^2$ is evaluated at the final stress state and initial temperature T_o, η_{mn} is the strain resulting from an externally applied stress σ_{rs} and β_{mn} are the thermal strain tensor defined by[7]

$$\beta_{mn} = (\partial \eta'_{mn} / \partial T)_{\sigma_{rs}} . \tag{67}$$

For the specific case of longitudinal waves propagating in an isotropic solid, we can express the thermal acoustic constants for the solids in the zero stress state as

$$[K_{11}]_{\sigma_{11} = 0,\, T = T_o} = [\frac{1}{2C_{11}} (\frac{\partial C_{11}}{\partial T})]_{\sigma_{11} = 0,\, T = T_o} \tag{68}$$

where we have used the defining equation (65) and the fact that $\rho_o W_L^2 = C_{11}$ for zero initial stress and initial temperature. Substituting equation (64), we obtain the expression for the thermal acoustic constant in terms of initial state parameters as

$$[K_{11}]_{\sigma_{11} = 0,\ T = T_o} = \frac{-\rho_o k_B}{4C_{11}} \left[\left(\frac{3\,C_{11} + C_{111}}{C_{11}} \right)^2 - \frac{5\,C_{111} + C_{1111}}{C_{11}} \right] \tag{69}$$

where all the elastic constants in equation (69) are defined with respect to the initial state (zero stress, initial temperature).

Experimentally, we are interested in the stress dependence of the thermal acoustic constant. Differentiating equation (66) with respect to applied stress σ_{rs}, we obtain

$$\frac{1}{\partial\sigma_{rs}} [K_q]_{T = T_o} = \frac{1}{2\rho_o W_q^2} \Big[2\, \frac{\partial C_{ijk\ell}}{\partial T}\, k_j\, k_\ell\, A_i\, A_k\, A_m\, A_n + \left(\frac{\partial C_{j\ell mn}}{\partial T} + \frac{\partial C_{ijk\ell mn}}{\partial T}\, A_i\, A_k \right) k_j\, k_\ell \Big]\, S_{mnrs} \tag{70}$$

where we have assumed that the thermal strain tensor β_{mn} is stress independent to a first order approximation and have used the compliance constants S_{mnrs} to transform η'_{mn} to σ_{rs}. Substituting equations (59) and (60) into equation (70), we obtain

$$\frac{\partial}{\partial\sigma_{rs}} [K_q]_{T = T_o} = \frac{-\rho_o k_B}{2\rho_o W_q^2} \Big\{ 2 \sum_{s=1}^{3N} \left(\frac{\partial\gamma^s_{ij}}{\partial\eta_{k\ell}} \right)_{T_o} k_j k_\ell A_i A_k A_m A_n + \Big[\sum_{s=1}^{3N} \left(\frac{\partial\gamma^s_{j\ell}}{\partial\eta_{mn}} \right)_{T_o} + \sum_{s=1}^{3N} \left(\frac{\partial^2\gamma^s_{ij}}{\partial\eta_{k\ell}\partial\eta_{mn}} \right)_{T_o} A_i\, A_k \Big] k_j\, k_\ell \Big\}\, S_{mnrs}$$

$$= \text{Constant}\ . \tag{71}$$

Equation (71) relates the thermal acoustic constants to the strain generalized Grüneisen parameters which are fundamental parameters of the Debye solid. Following the theory of Garber and Granato,[26] the first strain derivatives of γ^s_{ij} involve fourth order elastic constants and the second derivatives of γ_{ij}^{s} involve fifth order elastic constants. This result provides a potential method to measure the fifth order elastic constants from the stress derivatives of the thermal acoustic constants. There is currently no technique available to the author's knowledge for such a measurement.

Equation (71) results directly from the fact that expansions of the acoustic natural velocity with respect to temperature and stress is adquately represented for our range of experimental conditions by retaining only linear term.

III. EXPERIMENTAL TECHNIQUES

1. Measurement considerations

In order to verify the theoretical derivations, both pulse echo and a gated continuous wave acoustic velocity measurement technique are used. Theoretically, the time domain broadband pulse measurements are equivalent to the frequency domain continuous wave measurements since they are related to each other through a Fourier transformation. The accuracy of the acoustic wave measurements is affected and limited by such physical phenomena as wave dispersion, phase cancellation, ultrasonic attenuation, mode conversion, diffraction, and the effects of bonded transducers. The principal measurement errors result from mode conversion, diffraction, and the effects of bonded transducers. We shall discuss each of these primary sources of error separately.

A. Mode conversion

Mode conversion results from boundary effects on the transmission of the acoustic wave.[28] Consider the case of a longitudinal wave propagating along the axial direction of cylindrically shaped solid. The angle measured with respect to the axial direction at which mode conversion occurs is[29]

$$\theta = \sin^{-1} (V_S/V_L) \tag{72}$$

where V_S and V_L are acoustic shear and longitudinal wave velocity respectively. The time of arrival of the mode converted wave is

$$t = \frac{2\, m\ell_1}{V_L} + (n - 1)\, D \left(\frac{V_L^2 - V_S^2}{V_L\, V_S}\right)^{\frac{1}{2}}$$

where m, n are integers and D is the diameter of the sample. In the frequency domain, the effect of the mode converted wave is to modulate the spectra as shown in figure 1. The minimum in the modulation (cancellation) occurs whenever the coincident longitudinal wave and mode converted wave are π radians out of phase. The minimum occurs when the ultrasonic frequencies satisfy the equation

$$f_p = \frac{(2p + 1)\ V_L\ V_S}{nD(V_L^2 - V_S^2)^{\frac{1}{2}}} \tag{74}$$

where $p = 0, 1, 2 \ldots .$ Continuous wave measurements of frequency shifts near the cancellation points are subjected to error caused by the superposition of the mode converted waves.

The modulation of the spectra resulting from mode conversion nearly disappears at higher frequencies because of diminishing diffraction of the acoustic beam. The angle subtended by an acoustic beam measured with respect to the propagation direction is

$$\phi = \sin^{-1}\ (1.22\ \lambda/a) \tag{75}$$

where a is the diameter of the transducer and λ is the wavelength of the incident wave. For high frequencies, the angle decreases and less acoustic wave energy strikes the cylinder walls to be mode converted.

B. Diffraction

Because of the finite size of the transducer, the acoustic wave radiated from the transducer spreads out into a diffraction field with an angle ϕ described in equation (75). The diffraction effect is especially large for low frequencies and small transducers. The

Figure 1.- Effect of mode converted waves on the spectrum of a cylindrical resonator

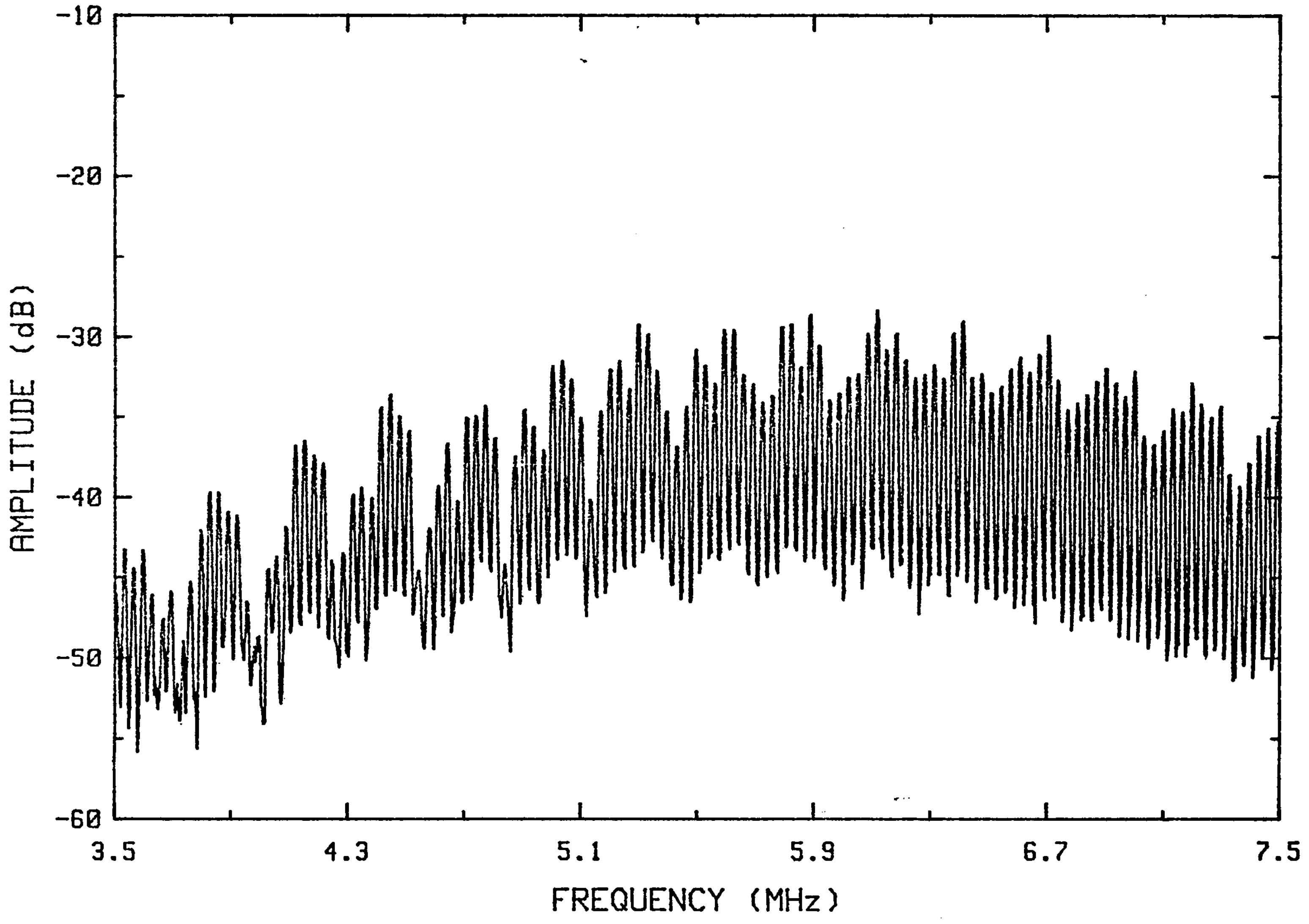
-10
-20
-30
-40
-50
-60
AMPLITUDE (dB)
3.5
4.3
5.1
5.9
6.7
7.5
FREQUENCY (MHz)

The intensity at distance d in the sample along the axis of the transducer is shown to be[30]

$$I = I_o \sin^2 \{\pi/\lambda\ [(a^2 + d^2)^{\frac{1}{2}} - d\ ]\ \} \tag{76}$$

where I_o is the maximum value of I. The response of a typical piston source is shown as a function of intensity I and distance d in figure 2. The spacing of the peaks increases with distance from the transducer. The region between the transducer and the position of the final intensity maximum occurring at approximately $d = 1.05\ a^2/\lambda$ is described as the Fresnel zone. Beyond the Fresnel zone lies the Fraunhofer zone. The intensity in the Fraunhofer zone falls off with the inverse square of the propagation distance as can be seen from equation (76) when $d \to \infty$

$$I\ \alpha\ (\pi a^2/2\lambda d)^2 \tag{77}$$

The diffracted wave in the Fraunhofer zone contains energy removed from the axial direction. When the diffracted wave is reflected at the lateral boundaries of the sample back into the main beam phase cancellation of the superimposed wave may be observed. Thus, the measurements are confined to the Fresnel zone to minimize such effects.

In the Fresnel zone, the intensity variation obtained by integrating the incident acoustic wave across the face of the receiving transducer introduces error in pulse time-of-flight measurements of the ultrasonic velocity. A detailed correction is given by Rogers and Van Buren.[31]

C. Effect of bonded transducers

For both conventional pulse and continuous wave (CW) measurements of acoustic wave velocity, the presence of the transducer and coupling

Figure 2.- Variation of acoustic intensity I with distance resulting from diffraction

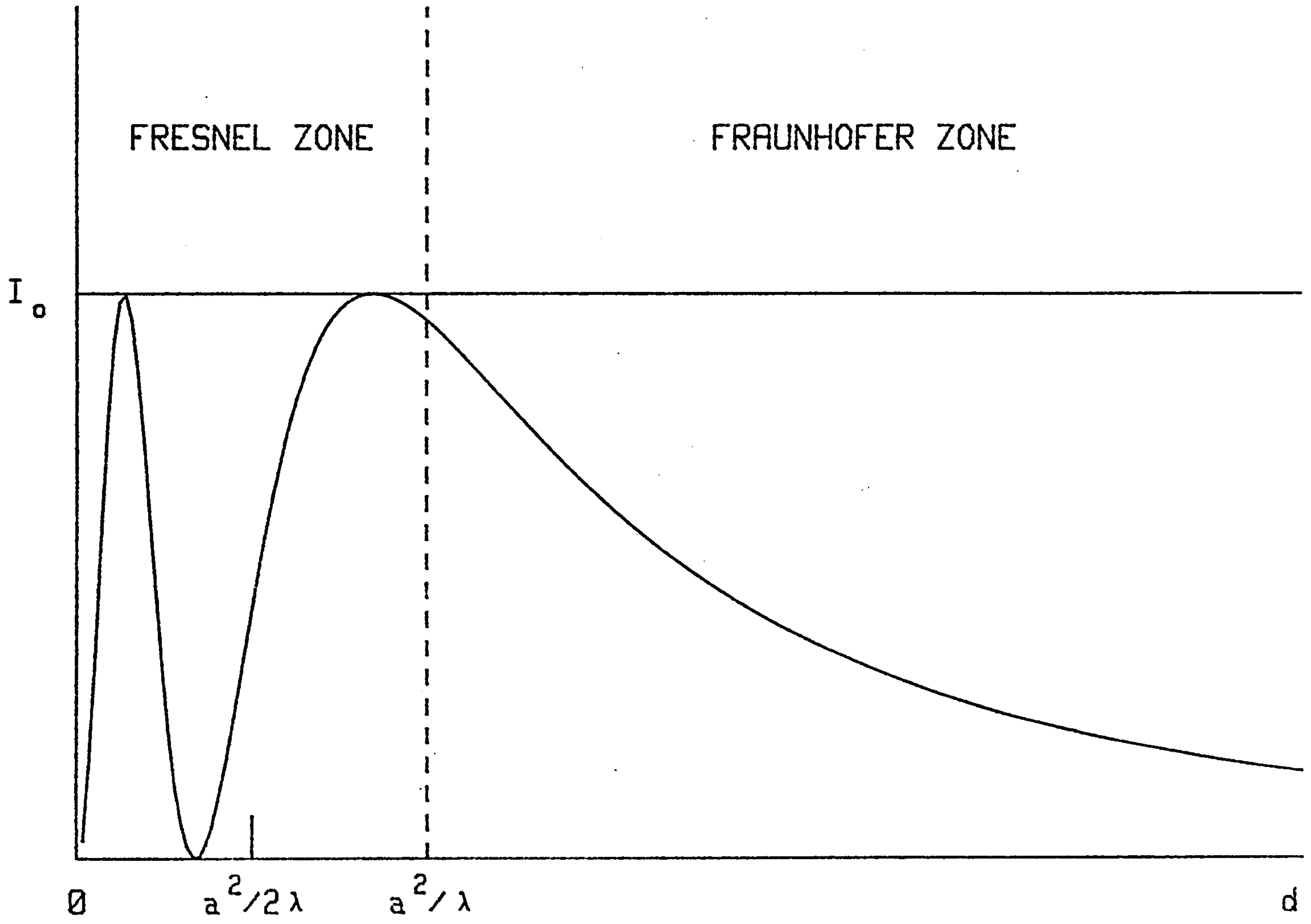
FRESNEL ZONE
FRAUNHOFER ZONE
I_o
0
$a^2/2\lambda$
a^2/λ
d

bond for solids induce errors in the velocity measurements of the sample. For pulse techniques, the transducer and bond errors are of the order of a few percent. The correction of the measurements are described by Papadakis[32] and McSkimin.[33]

For continuous wave measurements, the transducer and coupling bond produces shifts in standing wave resonance frequencies of the solid in a complicated manner. However, one can correct the measurements using the theory described by Bolef and Miller,[21] Ringermacher, Moerner and Miller[34,35] and the improved formulas derived by Chern, Cantrell, and Heyman,[36] and Chern, Cantrell, Heyman, and Winfree.[37] The detailed derivation and experimental verification of the new correction formula for standing wave acoustic phase velocity measurements including the effect of the coupling bond are fully described in Appendix.

An alternative approach is the use of noncontacting driver - capacitive receiver transducers. The capacitive system satisfied free - free boundary conditions and no bond corrections are required. The sample is set on the electrically grounded portion of a hollow ring assembly. The capacitive detector button is centered in the ring assembly and is recessed approximately 10 micrometers so that the electrode and sample face form a parallel-plate capacitor. The electrically isolated detector electrode is dc biased at approximately 110 V. The ultrasonic vibration of the sample face varies the gap spacing and generates an electrical signal.

In the capacitive driver, a 5-micrometer thick teflon spacer is placed between the capacitive driver and the sample face. A pulsed sinusoidally varying rf voltage is applied across the electrodes. Ultrasonic waves are generated in the sample from the electrostatic forces acting on the sample surface. The ultrasonic wave generated in the sample is produced at twice the frequency of the rf voltage applied to the driver. The detailed description of the capacitive system is given by Cantrell and Breazeale.[38]

A modification of the capacitive system is made by impedance matching the capacitive detector following the suggestion of Conradi.[39] The equivalent circuit of the capacitive detector and tuning circuit is shown in figure 3. The signal voltage V across the amplifier load resistance R is calculated to be

$$V = V_s \frac{1}{R + j\left(\omega L - \frac{1}{\omega C} - \frac{1}{\omega C_D}\right)} \tag{78}$$

where ω is the angular frequency, C_D is the quiescent capacitance of the detector, V_s is the signal source voltage, C is capacitance of the tuning capacitor and L is the inductance of the tuning inductor. When tuned at resonance, the signal voltage across the load R is equal to V_s.

Figure 3.- The equivalent circuit of the capacitive detector and tuning circuit.

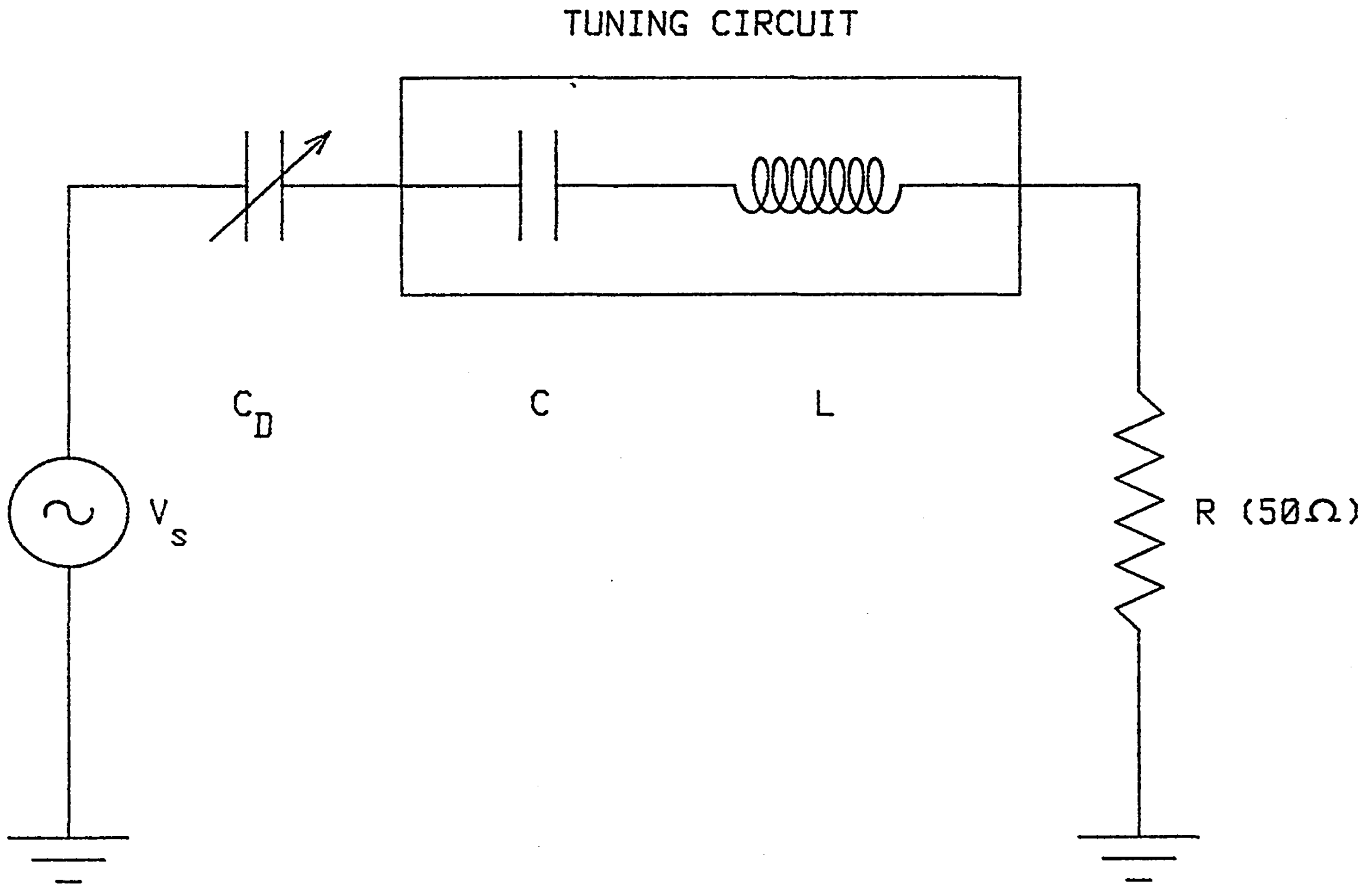
TUNING CIRCUIT
C_D
C
L
V_s
R (50Ω)

2. Measurement techniques

A. Pulse leading edge time-of-flight technique

In the pulse leading edge time-of-flight technique, one measures the time it takes a fast rise time pulse to traverse the sample. Since a pulse is used, this technique measures a group velocity rather than a phase velocity and as such is strongly influenced by attenuation and dispersion. For example, the higher frequencies of the pulse are more highly absorbed than are the lower frequency components. Thus, for some lossy samples, the initial start pulse may have a rise time orders magnitude faster than the stop pulse which must travel through the sample.

The pulse leading edge time-of-flight measurement uses a nanosecond risetime pulser and a pulse receiver to trigger the start and stop channels of universal time interval counter. A high risetime pulse ensures the start channel trigger on the very leading edge of the pulse. The received pulse is amplified to trigger the stop channel of the time counter.

B. Long-pulse frequency-tracking technique (Tone-burst spectroscopy)

In long-pulse tone-burst spectroscopy, a CW rf signal from a tracking generator is sent to a transmitter gate with an on-off ratio of 90dB. The gated rf pulse from the transmitter gate is amplified and the signal is used to drive a piezoelectric transducer. The transducer emits an ultrasonic pulse called a tone-burst having the same frequency as the CW source. The transmitter gate width is adjusted such that a standing wave equilibrium condition is established in the sample. In the equilibrium condition the wave energy input to the sample exactly balances the wave attenuation. The receiver gate width and position are adjusted by logic/timing generator such that signals are received only after the transmitter gate is turned off. The receiver rf signals are amplified and sent to the spectrum analyzer. As the tracking generator sweeps through range of frequencies, the spectrum analyzer continuously measures and displays a signal within a selected bandwidth at each frequency point in the sweep. Such an arrangement gives results equivalent to CW measurements without rf cross-talk problems inherent to CW measurements.[10,21] This technique can be used in one transducer reflection and two transducer transmission case. The block diagrams of the long-pulse frequency tracking tone-burst technique for reflection and transmission cases are shown in figure 4 and figure 5. The detail description of this frequency tracking tone-burst technique is given by Cantrell and Heyman.[10]

C. Pulsed phase locked loop spectrometer[11]

The pulsed phase locked loop spectrometer (P^2L^2) was developed for measuring changes in propagation phase velocity along a determined path length. This technique utilizes improvements on the basic scheme developed by Blume.[41] A gated tone-burst derived from a voltage controlled oscillator (VCO) is applied to a transducer as shown in figure 6. The acoustic wave generated propagates through the sample and is converted to an electrical pulse by a second transducer (or the same transducer for the reflection case). The signal is amplified and phase detected. The resulting signal is a voltage pulse of duration equal to the gate width and of amplitude determined by the phase relationship between the oscillator and the received ultrasonic pulse signal.

Figure 4.- Block diagram of the frequency tracking technique (tone-burst spectroscopy) for reflection configuration.

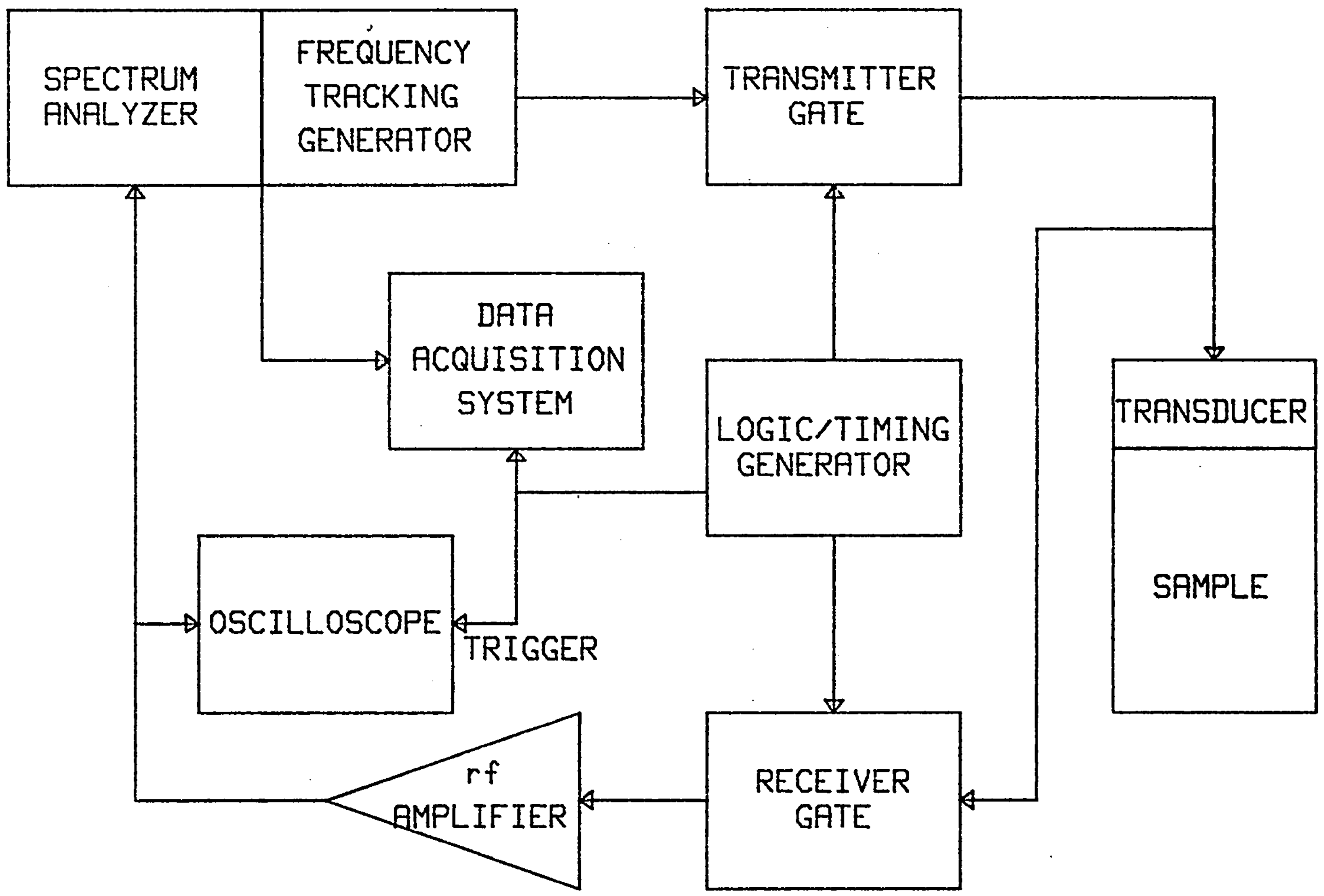
SPECTRUM ANALYZER
FREQUENCY TRACKING GENERATOR
TRANSMITTER GATE
DATA ACQUISITION SYSTEM
LOGIC/TIMING GENERATOR
TRANSDUCER
SAMPLE
OSCILLOSCOPE
TRIGGER
rf AMPLIFIER
RECEIVER GATE

Figure 5.- Block diagram of the frequency tracking technique for transmission configuration.

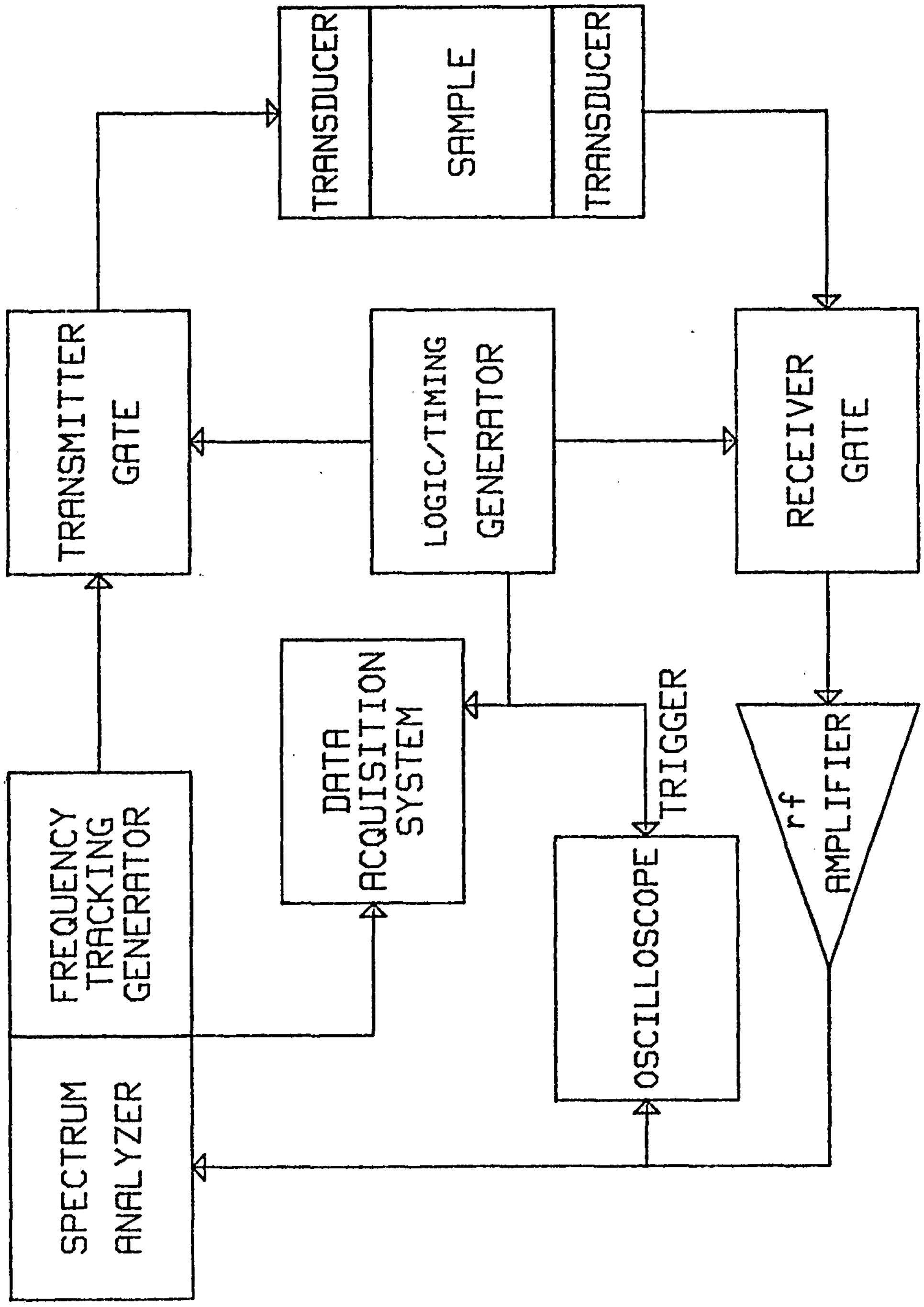

SPECTRUM ANALYZER
FREQUENCY TRACKING GENERATOR
TRANSMITTER GATE
TRANSDUCER
SAMPLE
TRANSDUCER
DATA ACQUISITION SYSTEM
LOGIC/TIMING GENERATOR
TRIGGER
OSCILLOSCOPE
RECEIVER GATE
rf AMPLIFIER

Figure 6.- Block diagram of the pulsed phase locked loop.

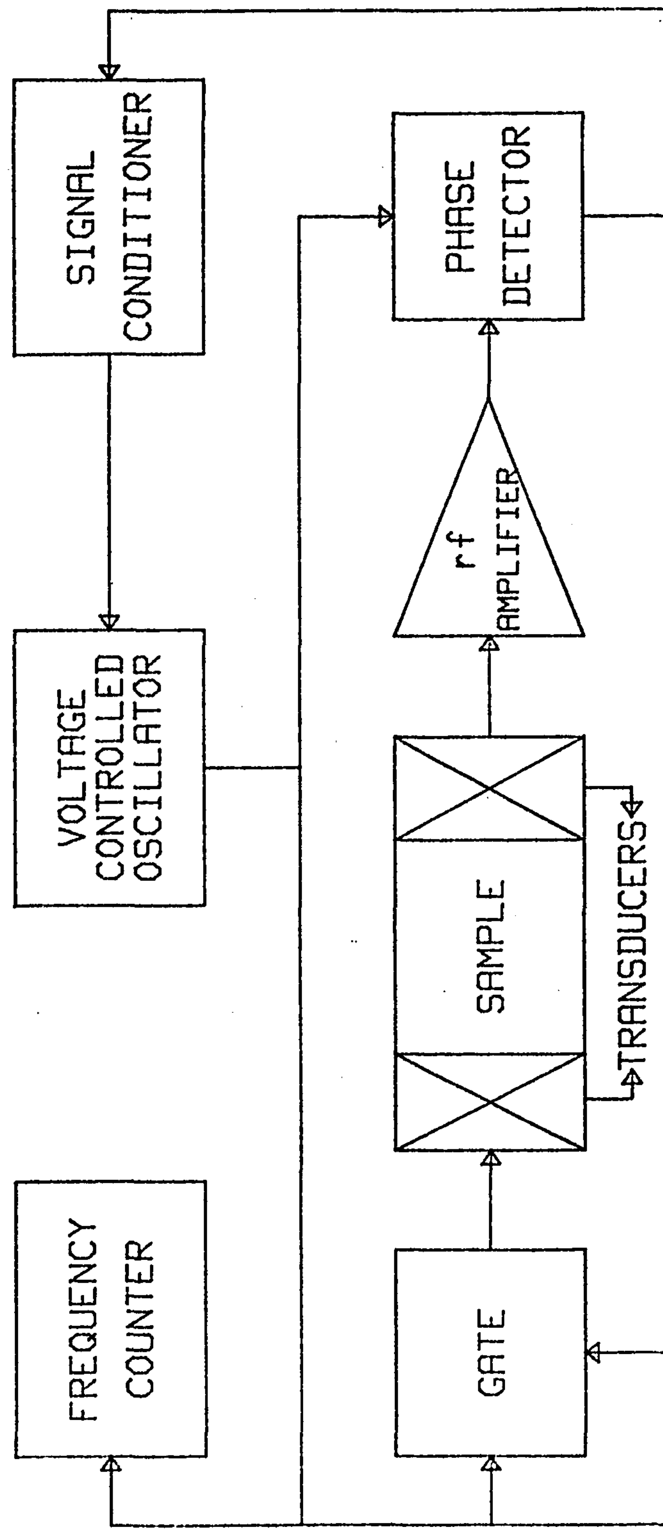
FREQUENCY COUNTER
VOLTAGE CONTROLLED OSCILLATOR
SIGNAL CONDITIONER
GATE
TRANSDUCERS
SAMPLE
rf AMPLIFIER
PHASE DETECTOR
DIVIDE NETWORK
LOGIC TIMING SYSTEM
SAMPLE/ HOLD

The voltage pulse is sampled and held on command from the logic timing generator. A control voltage generated by signal conditioning the sample/hold signal adjusts the rf frequency to maintain phase quadrature between an internal VCO and the chosen received acoustic pulse.

The acoustic phase shift ϕ which occurs in propagation through the sample with transit time t is: $\phi = 2\pi ft$ where f is the acoustic frequency. For the closed loop P^2L^2, ϕ is constant so that[20]

$$d\phi = 2\pi(tdf + fdt) = 0 \tag{79}$$

Thus,

$$\Delta f/f = -\Delta t/t \tag{80}$$

The mathematical result is the same as occurs from equation (49) with ℓ/V replaced by t. Therefore, the P^2L^2 has the equivalent dimensionless readout:

$$\Delta f/f = -\Delta t/t = \Delta V/V - \Delta\ell/\ell \tag{81}$$

where f, V and ℓ are the initial values and t is a final value. In contrast to the group velocity measurement of the pulse echo technique, the P^2L^2 measures a true phase velocity in the absence of velocity dispersion.

The stability and accuracy of the system requires that the sample/hold circuit have low droop rate to maintain a constant VCO frequency between update corrections. The feedback loop rate is limited by the sample attenuation since the acoustic energy in the sample should decay before a new gating sequence is begun. The measured short term stability of the P^2L^2 is approximately a part in 10^8 with temperature variation in the sample dominating the measured frequency variation. For our experiments, temperature stability limited the usable resolution to parts in 10^7. A detailed description of P^2L^2 is given elsewhere.[11]

3. Laboratory experiments

A. Stress acoustic measurements[20,41]

All samples used in the stress acoustic measurements were cylindrically shaped polycrystalline metals including aluminum 2024-T4, copper, phosphor bronze, titanium, mild steel, carbon steel and stainless steel. The samples were 2.54 cm in diameter, 30.5 cm in length and threaded on the ends to fit the sample holder. After preparation the samples were mounted in an MTS-810 material test system and axially loaded in tension incrementally from zero to 180 MPa in steps of 1 MPa. After each incremental increase in load the strain was measured with an MTS-632.13B extensometer placed on the sample surface midway between the planar ends. The change in the natural velocity of the sample was measured using the pulsed phase locked loop technique described in the previous section. It is shown in equation (50) that the P^2L^2 technique allows one to measure directly the change in the natural velocity by measuring the fractional change in the ultrasonic drive frequency.

A through-transmission leading edge time-of-flight technique is also used in parallel with the pulsed phase locked loop technique. A 20 picosecond resolution time interval counter was used in its interval statistics mode to average over several thousand pulses. Signals were amplified to saturation in a 1000-MHz bandwidth low noise amplifier to provide clean leading edges for the time interval counter. The block diagram of the stress acoustic measurements incorporated with thermal acoustic measurements will be presented in the next section.

B. Thermal acoustic measurements[9]

In order to verify the theoretical predictions in section 4 of Chapter II, laboratory experiments were performed using both pulsed phase locked loop and leading edge pulse time-of-flight measuring techniques. The sample used is a 30.462 cm long 2.54 cm diameter polycrystalline aluminum (2024-T4) rod. The block diagram of experimental set up is shown in figure 7. The aluminum sample is installed in an insulated over and is mounted in a MTS-810 material test system. An extensometer, a solid state thermometer and thermocouples are placed on the middle and ends of the sample surface. A 2.25 MHz gated rf tone-burst from the VCO of the P^2L^2 is transmitted via a PZT transducer to the sample. The acoustic signals are reflected from the end of the sample and received by the same transducer. As with the transmission P^2L^2 described earlier, a control voltage from the P^2L^2 VCO adjusts the rf frequency maintaining phase quadrature. The acoustic amplitude, phase signal, and the sampling position are displayed and monitored with an oscilloscope. In addition, the rf pulse is used to trigger the start channel of a universal time interval counter. A second transducer is bonded on the other end of the sample to receive the acoustic signal which is amplified and used to trigger the stop channel of the time counter. The experiments are performed by slowly heating up the aluminum sample from room temperature. The stress, strain, temperature, time of flight, and normalized frequency are recorded with a computer controlled data acquisition system. The experiments involve propagating 2.25 MHz longitudinal waves along the uniaxial tensile stress direction of a polycrystalline aluminum rod over a temperature range of $25^{\circ}C$-$65^{\circ}C$ and the stress range of 0-150 MPa. The amplitude and thus the pulse leading edge arrival time is affected by diffraction and attenuation which are functions of temperature and stress. The resolution of the leading edge time-of-flight technique is

Figure 7.- Block diagram of the thermal stress test system

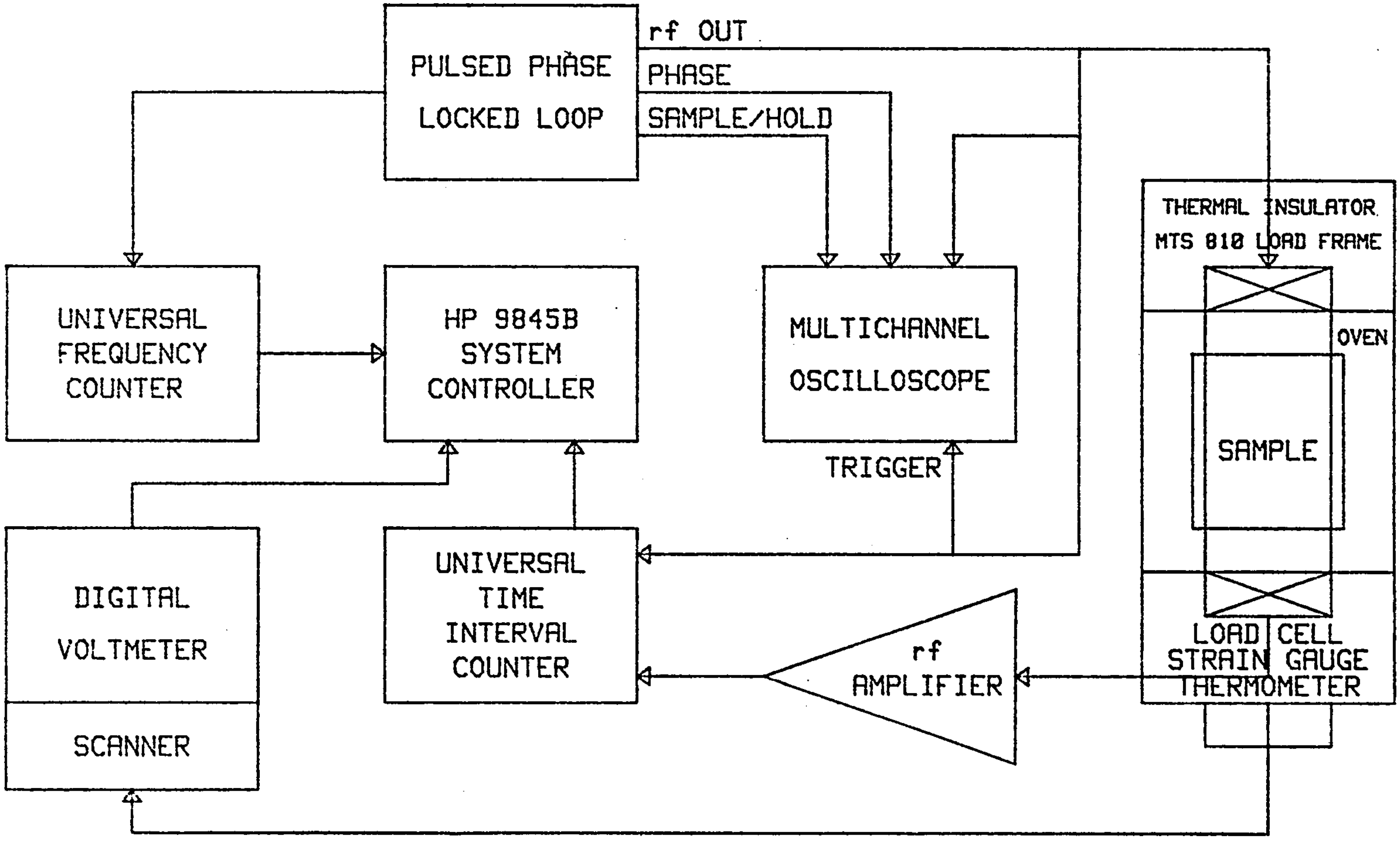
PULSED PHASE LOCKED LOOP
rf OUT
PHASE
SAMPLE/HOLD
UNIVERSAL FREQUENCY COUNTER
HP 9845B SYSTEM CONTROLLER
MULTICHANNEL OSCILLOSCOPE
TRIGGER
THERMAL INSULATOR
MTS 810 LOAD FRAME
OVEN
SAMPLE
LOAD CELL
STRAIN GAUGE
THERMOMETER
DIGITAL VOLTMETER
SCANNER
UNIVERSAL TIME INTERVAL COUNTER
rf AMPLIFIER

about one part in 10^5 in contrast to the pulsed phase locked loop resolution of parts in 10^7.

IV. RESULTS AND DISCUSSION

1. Axial stress measurements

The determination of axial stress using ultrasonic techniques involves material parameters shown in equation (51) combined with known changes in $\Delta f/f$. The stress acoustic constant contains elastic properties of the stressed material and varies from material to material.

Figure 8 shows a typical P^2L^2 stress-acoustic as well as stress-strain and stress-true velocity measurement of an aluminum 2024-T4 sample. The variation of stress acoustic constants for various materials is shown in figure 9. The slope of these curves represent stress acoustic constants H_{11} and are determined from the figure as: H_{11} aluminum = 5.38×10^{-5}/MPa; H_{11} titanium = 2.09×10^{-5}/MPa; H_{11} stainless steel = 2.33×10^{-5} MPa; H_{11} mild steel = 1.59×10^{-5}/MPa.

A factor which influences ultrasonic stress measurements is the percentage of sample under axial load. The details of percentage loading study is given elsewhere.[20] To eliminate the nonuniform tensile loading, the sample geometry was carefully selected without compromising diffraction effects.

Temperature also plays an interesting role in the stress acoustic measurements. For the case of aluminum 2024-T4, a small change in temperature such as 5°C will produce a corresponding $\Delta f/f$ of 10^{-3} or about 20MPa effective stress. A more subtle temperature effect involves the adiabatic temperature decrease resulting from the thermodynamic volume expansion. In figure 10, data are presented for temperature, strain and $\Delta f/f$ as a function of time for a step loading/unloading

Figure 8.- Typical stress-acoustic, stress-strain and stress-true velocity data for an aluminum sample.

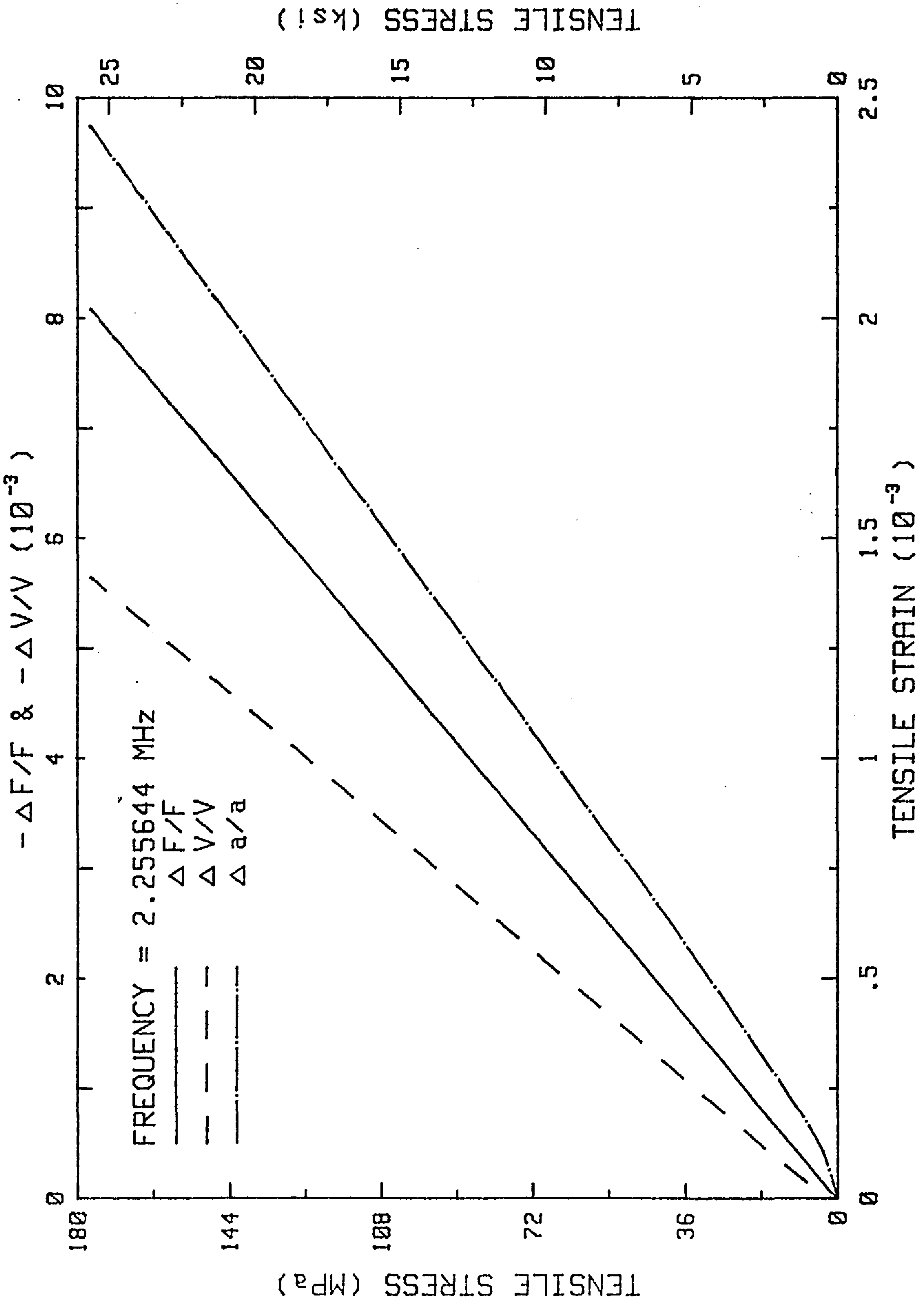

−ΔF/F & −ΔV/V (10^{-3})
0
2
4
6
8
10
FREQUENCY = 2.255644 MHz
ΔF/F
ΔV/V
Δa/a
TENSILE STRAIN (10^{-3})
0
.5
1
1.5
2
2.5
TENSILE STRESS (MPa)
0
36
72
108
144
180
TENSILE STRESS (ksi)
0
5
10
15
20
25

Figure 9.- Stress acoustic response for various materials.

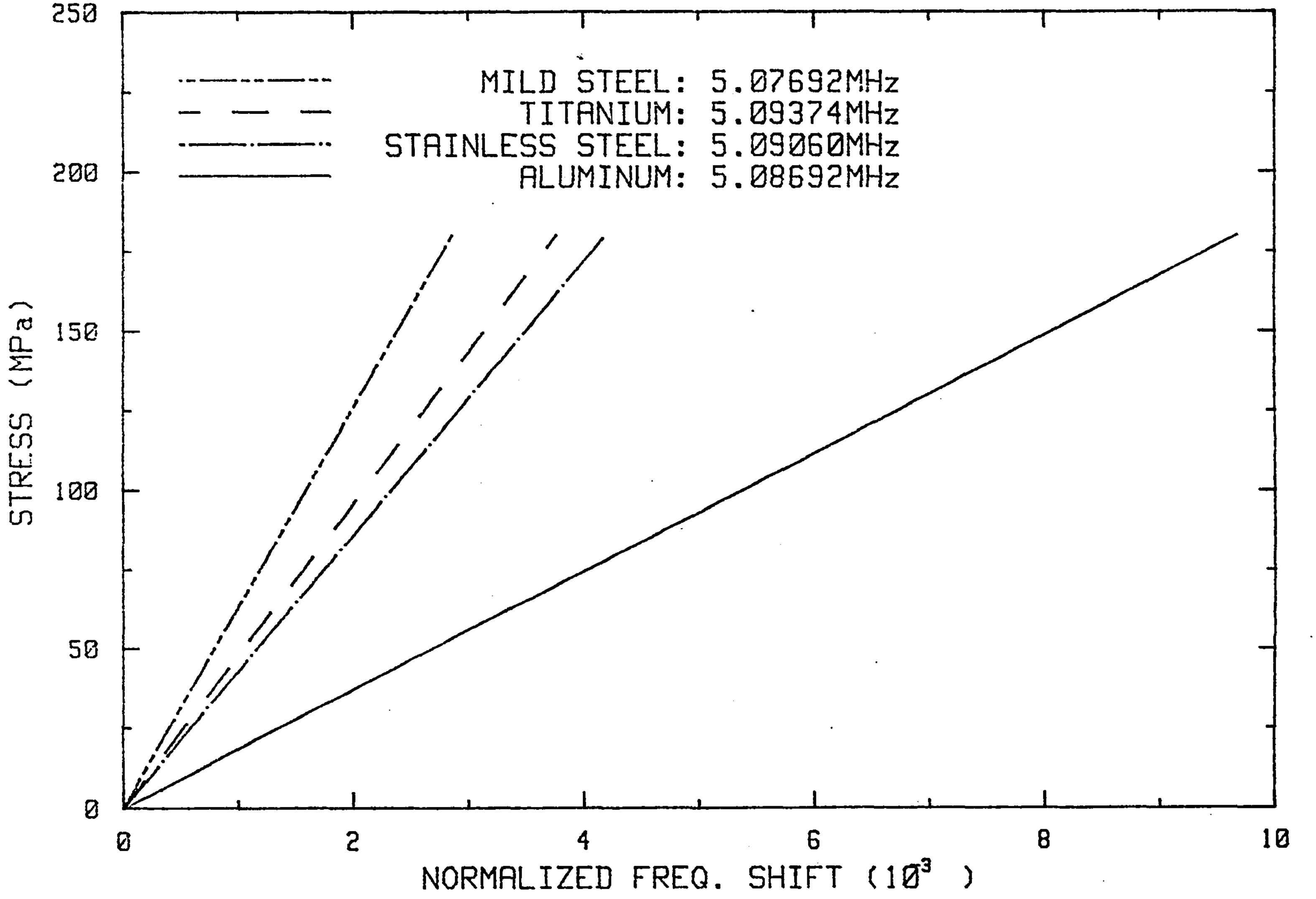

MILD STEEL: 5.07692MHz
TITANIUM: 5.09374MHz
STAINLESS STEEL: 5.09060MHz
ALUMINUM: 5.08692MHz
STRESS (MPa)
250
200
150
100
50
0
0
2
4
6
8
10
NORMALIZED FREQ. SHIFT (10³)

Figure 10.- Experimental data for temperature, strain and $\Delta f/f$ as a function of time for step loading/unloading of an aluminum sample.

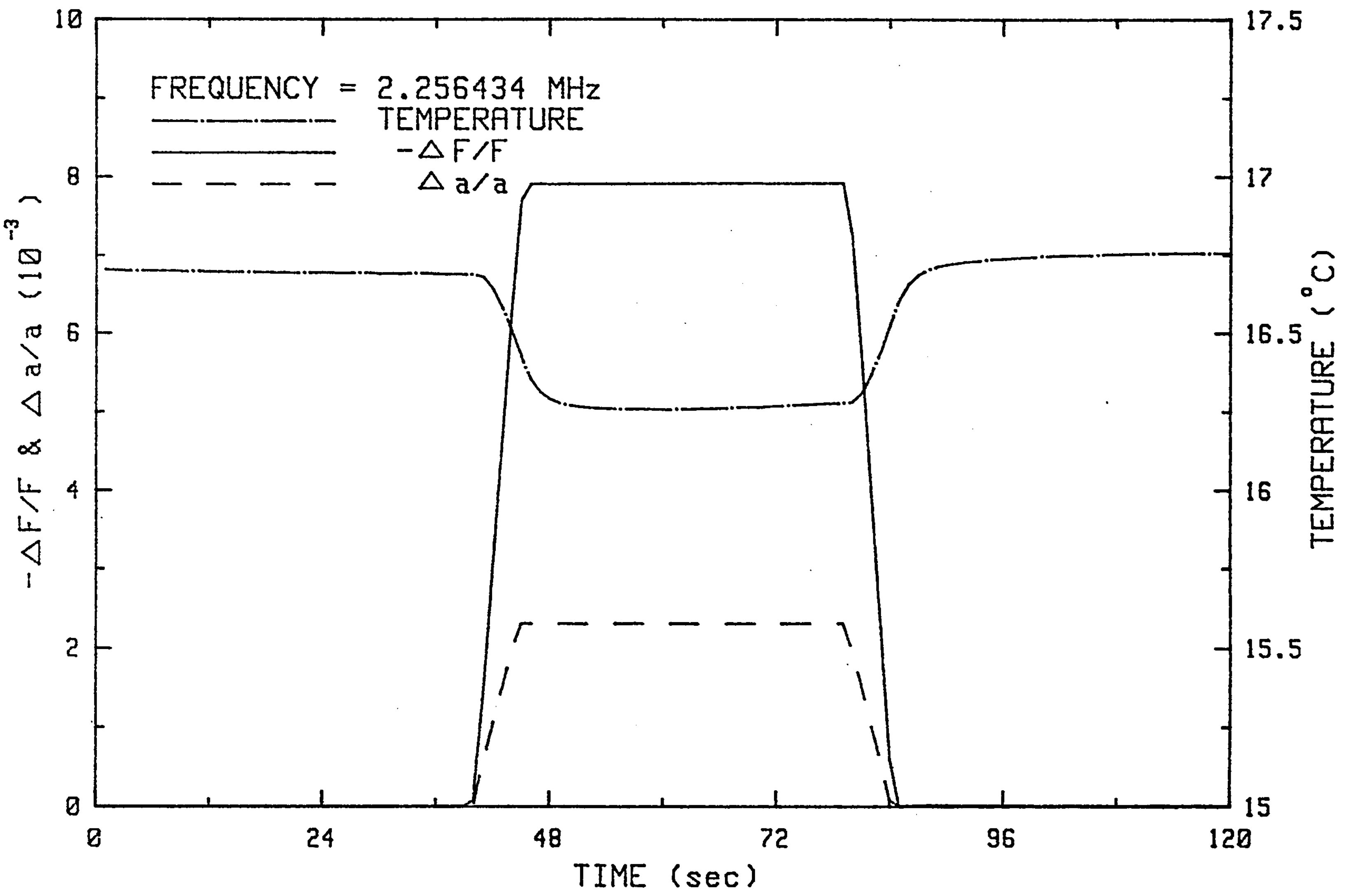
FREQUENCY = 2.256434 MHz
TEMPERATURE
-△F/F
△a/a
-△F/F & △a/a (10^-3)
TEMPERATURE (°C)
TIME (sec)
0
2
4
6
8
10
15
15.5
16
16.5
17
17.5
0
24
48
72
96
120

of the aluminum sample. The temperature drop of $1^{o}C$ resulted from a 125 MPa tensile stress. This result is similar to the sample expansion of a gas and its subsequent cooling.

2. Thermal acoustic stress measurements

Typical experimental data of normalized frequency change with respect to changes in temperature for an applied stress is shown in figure 11. The thermal acoustic constants K_{11} are obtained by a linear curve fitting routine for each thermal stress experiment. Thermal measurements were obtained for six stress levels. The plot of thermal acoustic constants as a function of stress is shown in figure 12. The sample cooled slowly until it reached equilibrium with room temperature. The data is also linearly curve fitted to obtain the stress derivative of the thermal acoustic constants which is the slope of the curve. The stress derivative of the thermal acoustic constants $\Delta K_{11}/\Delta\sigma_{11}$ is found to be $7.780 \times 10^{-7}/\mathrm{MPa}^{o}\mathrm{C}$.

Figure 12 presents data showing a linear relationship between the applied stress and thermal acoustic constant. This result verifies the theoretical assumption upon which the experiment was based.

Similar experiments performed by Salama and Ling[42] also show a linear relationship between applied stress and the thermal acoustic constants. Table 1 presents Salama and Ling's data for compressional stress applied perpendicular to the longitudinal wave propagation in aluminum samples. They present data as a change in real velocity ΔV per degree K for three aluminum 2024 samples. For all samples, the application of stress decreased $\Delta V/\Delta T$ with higher value of stress producing a larger decrease.

Figure 11.- Typical experimental data of normalized frequency change with respect to temperature.

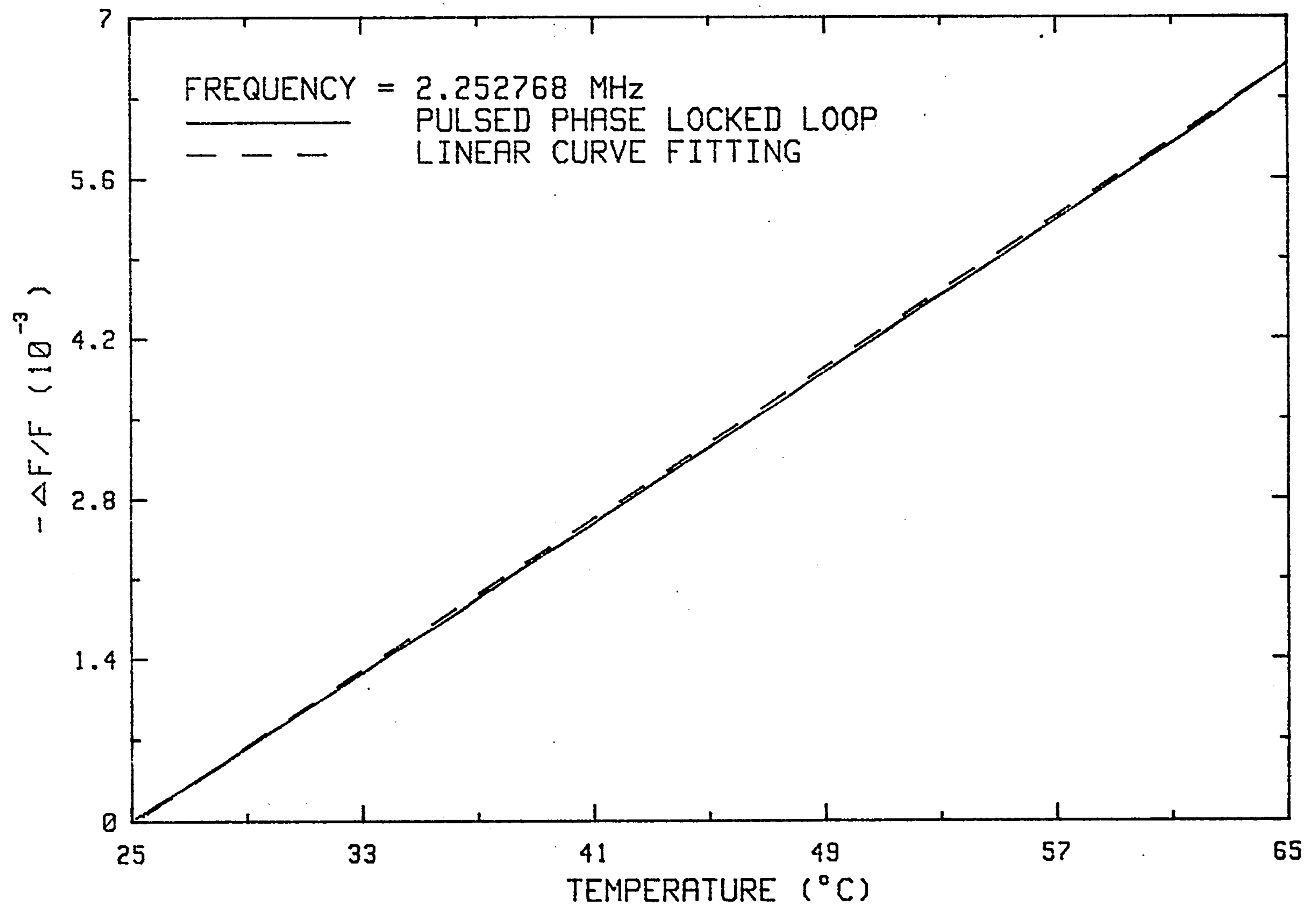
FREQUENCY = 2.252768 MHz
PULSED PHASE LOCKED LOOP
LINEAR CURVE FITTING
7
5.6
4.2
2.8
1.4
0
$-\Delta F/F\ (10^{-3})$
25
33
41
49
57
65
TEMPERATURE (°C)

Figure 12.- Thermal acoustic constants shown as a function of material stress.

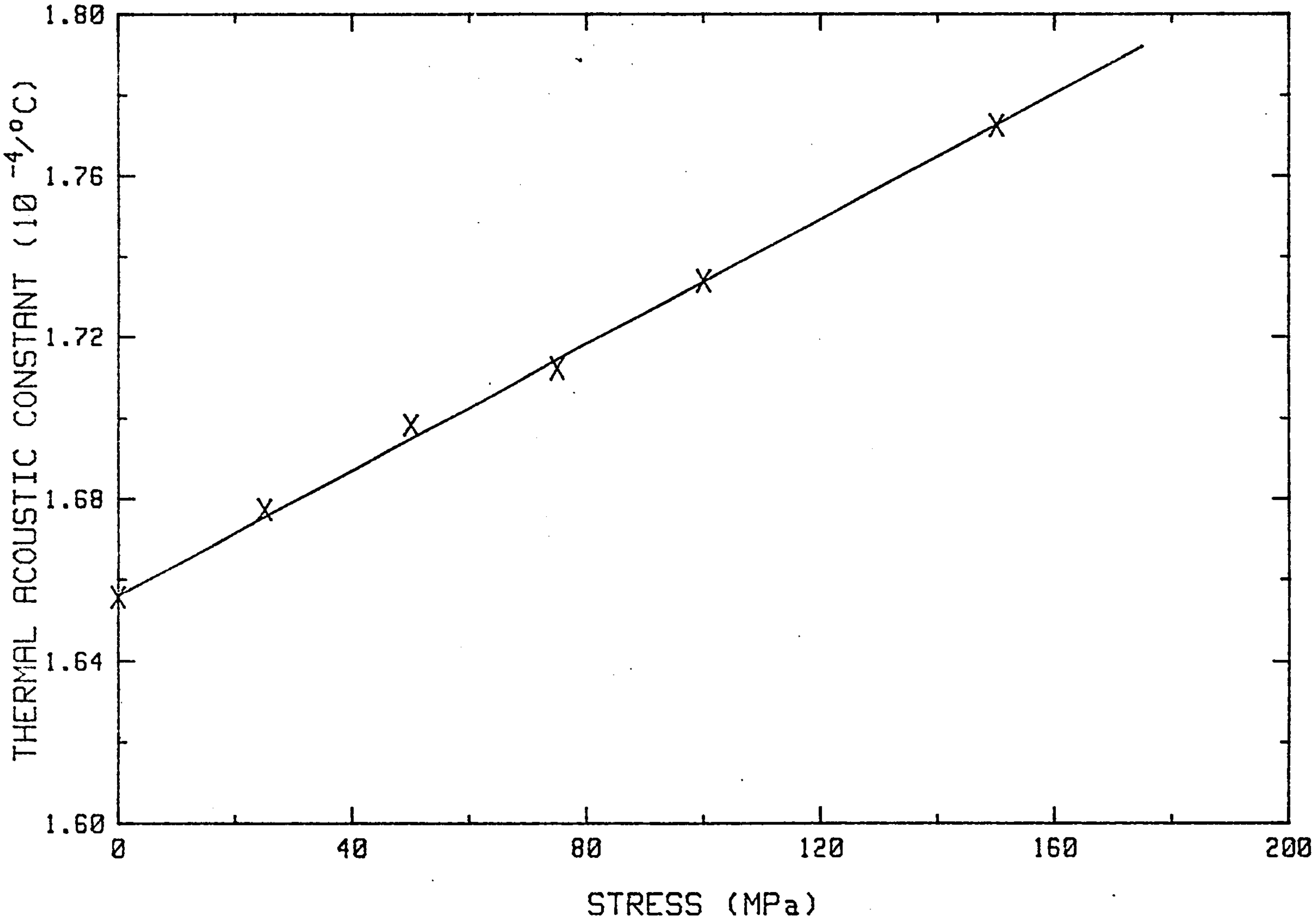
1.80
1.76
1.72
1.68
1.64
1.60
THERMAL ACOUSTIC CONSTANT (10 $^{-4}$/°C)
0
40
80
120
160
200
STRESS (MPa)

The present experimental results are shown in Table 2 for tensile stress applied along the direction of wave propagation. The change in normalized natural velocity $\Delta f/f$ per degree C is the measurement parameter chosen from the theoretical results. For an aid on comparison with Salama and Ling's results, the values were transformed into the representation $-\Delta V/\Delta T$. It is interesting to note that our value for the zero stress slope of 0.927 m/sec^{o}C is in close agreement with that of Salama and Ling's 0.923 m/sec^{o}K for the "A" sample. Variation in the zero value reported by Salama and Ling may be caused by sample differences (such as texture of residual stress).

In summary, a theoretical model has been developed predicting a linear dependence of the slope of the thermal acoustic constants with material stress. The experimental results confirm the model and present new directions for further inquiry.

TABLE I

EXPERIMENTAL RESULTS OF SALAMA AND LING. COMPRESSIONAL STRESS IS APPLIED IN THE DIRECTION PERPENDICULAR TO WAVE PROPAGATION.

Specimen	Applied Compressional Stress (MPa)	$-\Delta V/\Delta T$ ($m \cdot s^{-1} \cdot K^{-1}$)
A (2024-0)	0.0	0.923
	21.4	0.878
B (2024-0)	0.0	0.957
	37.2	0.856
C (2024-0)	0.0	1.007
	44.1	0.908

TABLE 2

PRESENT EXPERIMENTAL RESULTS. TENSILE STRESS IS APPLIED ALONG THE DIRECTION OF WAVE PROPAGATION.

Specimen	Applied Tensile Stress (MPa)	$-(\Delta f/f)/\Delta T$ ($10^{-4}/^{o}C$)	$-\Delta V/\Delta$ ($m\cdot s^{-1}\cdot {}^{o}C^{-1}$)
aluminum 2024-T4	0	1.654	0.927
	25	1.674	0.938
	50	1.697	0.949
	75	1.713	0.957
	100	1.734	0.966
	150	1.772	0.988

3. Relative slope invariance of velocity-stress and strain-stress curves

Recent studies of residual stress in materials have led us to measure simultaneously the natural velocity and the strain in several polycrystalline metals as a function of applied stress. We find that the curves are approximately linear and that the ratios of the slope of the velocity-stress curve to the slope of the strain-stress curve for the materials cluster around = -3.5:1. The values are R = -3.5 for aluminum 2024-T4; R = -2.9 for carbon steel; R = -3.6 for mild steel; R = -2.9 for copper; R = -2.8 for phosphor bronze. The difference is surprisingly small when one considers the large variation in mechanical properties of the material measured.

We examine the results from the thermoelastic theory in terms of independent measurements of second and third order elastic constants. The fractional change in the natural velocity W of a solid per unit change in externally applied uniaxial stress of magnitude P in unit direction $\hat{n}$ is

$$\frac{1}{W}\frac{\partial W}{\partial P} = \frac{1}{W}\frac{\partial W}{\partial \sigma_{rs}} n_r n_s \tag{82}$$

where the general stress tensor

$$\sigma_{rs} = P n_r n_s \tag{83}$$

and n_i are the Cartesian components of $\hat{n}$. Using the results of equation (41), we may write

$$\begin{aligned}\frac{1}{W}\frac{\partial W}{\partial P} = \frac{1}{2\rho_o W^2} & (C_{j\ell mn} + C_{ijk\ell mn} A_i A_k) k_j k_\ell S_{mnrs} n_r n_s \\ & + S_{mnrs} A_m A_n n_r n_s \end{aligned} \tag{84}$$

where the derivative is evaluated in the zero stress configuration.

The free Young's modulus E_f in direction $\hat{n}$ of a solid is defined as the ratio of tensile stress P to the resulting linear strain η in the solid. The free modulus can be expressed in terms of the compliance coefficients as[43]

$$\frac{1}{E_f} = S'_{1111} = \frac{\eta}{P} \tag{85}$$

In equation (85)

$$\eta = \eta_{ij}\, n_i\, n_j \tag{86}$$

where η_{ij} are the components of the strain tensor and S'_{1111} is the (1111) component of the compliance tensor defined in a (primed) coordinate system appropriately rotated with respect to a fixed (unprimed) coordinate system in the solid. Let the transformation from the unprimed to the primed coordinate system be defined by the transformation tensor

$$R_{ij} = \begin{pmatrix} n_1 & n_2 & n_3 \\ m_1 & m_2 & m_3 \\ \ell_1 & \ell_2 & \ell_3 \end{pmatrix} \tag{87}$$

The compliance tensor transforms as

$$S'_{ijk\ell} = R_{im}\, R_{jn}\, R_{kp}\, R_{\ell q}\, S_{mnpq} \tag{88}$$

Hence,

$$S'_{1111} = \frac{1}{E_f} = S_{mnpq}\, n_m\, n_n\, n_p\, n_q. \tag{89}$$

If we assume the wave polarization $\hat{A}$ of applied stress, then $A_i = n_i$ in equation (84). If we further assume pure mode propagation, then $k_i = n_i$ and the ratio R of the natural velocity-stress slope to the strain stress slope is

$$R = \frac{1}{W}\,\frac{\partial W}{\partial P}\Big/\frac{n}{P} = 1 + \frac{E_f}{2\rho_o W^2}\,(C_{j\ell mn}\, S_{mnrs}\, n_j\, n_\ell\, n_r\, n_s + C_{ijk\ell mn}\, S_{mnrs}\, n_i\, n_j\, n_k\, n_\ell\, n_r\, n_s). \tag{90}$$

Using the relation of equation (39), equation (90) becomes

$$R = 1 + \frac{E_f}{2\rho_o W^2}\,(1 + C_{ijk\ell mn}\, S_{mnrs}\, n_i\, n_j\, n_k\, n_\ell\, n_m\, n_n) \tag{91}$$

For longitudinal waves propagating in an isotropic solid along the direction of applied stress, equation (91) reduces to

$$R = 1 + \tfrac{1}{2}\, C_{111}/C_{11} + \frac{1 + C_{112}\, S_{12}}{2\, S_{11}\, C_{11}} \tag{92}$$

where we have contracted the indices of the elastic coefficients by using Voigt notation.

Using equation (92) and the values of the elastic coefficients obtained from the literature,[44-46] we calculate R for a number of isotropic materials. These calculations along with the present R values data are listed in Table 3.

With two exceptions (Austenitic steel and fused silica) the R value fall in the range -2.7 to -3.9 even though the elastic coefficients of those materials in that range vary more than 700%. The reason for the unusually large negative R value for Austenitic steel (R = -6.2) is not clear but may be related to the crystalline structure

TABLE 3

R VALUES OF ISOTROPIC MATERIALS CALCULATED FROM ELASTIC COEFFICIENTS AND FROM PRESENT WORK

Material	R value	Reference
Rail Steel	-3.5	44
Hecla 37 Steel	-3.9	45
Hecla 17 Steel	-3.5	45
Hecla 138A	-3.8	45
Rex 535	-3.4	45
Mild Steel	-3.6	present work
Carbon Steel	-2.9	present work
Hecla ATV Austenitic	-6.2	45
Aluminum 2024-T4	-3.5	present work
Magnesium	-3.9	45
Molybdenum	-2.9	45
Tungsten	-2.7	45
Copper	-2.9	present work
Phosphor Bronze	-2.8	present work
Fused Silica	+4.9	46

of the grains. The grains of Austenitic steel have a fcc structure whereas the grains of the other steel alloys exhibit a bcc structure.

The sign of R for fused silica is positive ($R = +4.9$) in contrast to the other solids listed. The positive value of R is directly related to the fact that the third order elastic constants of fused silica are dominantly positive whereas for all other materials listed are dominantly negative. Fused silica, unlike the "quasi-isotropic" polycrystalline metals, has an isotropic amorphous structure consisting of a network of partly ionic-partly covalent SiO_4 tetrahedra having short-range but not long-range order. This arrangement gives rise to a number of anomalous properties of fused silica including a large negative thermal expansivity at low temperature[47] and a double potential well.[48] White and Birch[49] suggest that such properties may be the result of transverse vibrations associated with the oxygen atoms of the tetrahedral network. Measurements by Cantrell and Breazeale[50] of the longitudinal mode strain generalized Grüneisen parameters of fused silica as a function of temperature give results consistent with this assumption.

APPENDIX

Improved formula for CW measurements of ultrasonic phase velocity using one transducer[36]

1. Theory

Consider a one-dimensional compound resonator consisting of a transducer bonded to a solid sample. The properties of the compound resonator are labeled with the subscript c. The subscripts s, t and b designate the properties of the sample, transducer, and bond, respectively. We seek to determine the velocity of sound in the sample V_s from measured CW resonance frequencies f_c^m (m = integer) of the compound resonator.

Transmission line theory predicts that for lossless propagation media, the resonance frequencies of the compound resonator occur at the roots of the transcendental equation[21]

$$Z_s \tan k_s \ell_s + Z_t \tan k_t \ell_t + Z_b \tan k_b \ell_b - (Z_s Z_t/Z_b) \tan k_s \ell_s \tan k_t \ell_t \tan k_b \ell_b = 0 \tag{A-1}$$

where k is the wave number and ℓ is the thickness of the medium. The acoustic impedance $Z = \rho V$, where ρ is the density and V is the sound velocity of the medium. Although equation (A-1) can be solved numberically for V_s with the aid of a computer, we wish to obtain an approximate but explicit solution for V_s, which is more accurate than previous solutions but which also lends itself to calculation using equipment less sophisticated than a computer.

The problem can be greatly simplified by initially neglecting the contribution of the bond to the compound resonator. The effect of the bond will be considered later. Setting to zero the terms in equation (A-1) involving the bond, we obtain the equation

$$Z_s \tan k_s \ell_s + Z_t \tan k_t \ell_t = 0 \tag{A-2}$$

It is convenient to rewrite equation (A-2) in a form which emphasizes the frequency differences between adjacent mechanical resonances rather than the resonance frequencies themselves. The mechanical resonances of the isolated sample occur at frequencies $f_s^s = mV_s/2\ell_s$ (m = integer) while the fundamental resonance of the isolated transducer occurs at $f_t = V_t/2\ell_t$. The frequency differences between adjacent mechanical resonances of the compound resonator are written as $\Delta f_c^m = f_c^{m+1} - f_c^m$ and of the isolated sample as $\Delta f_s^m = f_s^{m+1} - f_s^m$. Although Δf_c^m varies with the choice of m, Δf_s^m is independent of m, and we may write

$$\Delta f_s = \Delta f_s^m = V_s/2\ell_s = f_s^m/m.$$

If we write equation (A-2) for each of two adjacent resonances and employ the trigonometric identities $\tan(\alpha - \beta) = (\tan\alpha - \tan\beta)/(1 + \tan\alpha \tan\beta)$ and $\tan(\alpha - \pi) = \tan\alpha$, we obtain, after substantial algebraic manipulation, the equation

$$\tan \pi \left(\frac{\Delta f_c^m - \Delta f_s}{\Delta f_s}\right) = \frac{-\Delta f_s B}{(\Delta f_s)^2 + A} \tag{A-3}$$

where

$$A = \delta^2 (f_t)^2 \tan \frac{\pi f_c^{m+1}}{f_t} \tan \frac{\pi f_c^m}{f_t} \tag{A-4}$$

$$B = \delta f_t \left(\tan \frac{\pi f_c^{m+1}}{f_t} - \tan \frac{\pi f_c^{m}}{f_t}\right) \tag{A-5}$$

and

$$\delta \equiv \rho_t\, \ell_t / \rho_s\, \ell_s\,. \tag{A-6}$$

δ is a parameter that was originally introduced by Bolef and Menes[51] and later used by Ringermacher et. al.[34] to characterize the dominant experimentally controlled variables. It must be pointed out that δ is a function of the sample and transducer densities and lengths. In this context changes in δ were assumed to result from changes in the sample length only for a given set of densities and transducer thickness.

Since the argument of the tangent function in equation (A-3) is small, we can approximate the tangent function by its argument to obtain

$$\Delta f_s \left[(\Delta f_s)^2 - \left(\frac{B}{\pi} + \Delta f_c^m\right) \Delta f_s\right] + A\, \Delta f_s - A\, \Delta f_c^m = 0 \tag{A-7}$$

An accurate approximation to equation (A-7) can be obtained by setting the first Δf_s term in the expansion to Δf_c^m. Making this substitution, we get

$$\Delta f_c^m \left[(\Delta f_s)^2 - \left(\frac{B}{\pi} + \Delta f_c^m\right) \Delta f_s\right] + A\, \Delta f_s - A\, \Delta f_c^m = 0 \tag{A-8}$$

Solving equation (A-8) for Δf_s and using the relation $V_s = 2\ell_s\, \Delta f_s$ we obtain an explicit expression for V_s in the form

$$V_s \simeq \ell_s \left\{\Delta f_c^m + \frac{B}{\pi} - A\,(\Delta f_c^m)^{-1} \pm \left[\left(\Delta f_c^m + \frac{B}{\pi} - A(\Delta f_c^m)^{-1}\right)^2 + 4A\right]^{\frac{1}{2}}\right\} \tag{A-9}$$

where A and B are given by equations (A-4) and (A-5). The experiments reported here indicate that the plus sign in equation (A-9) is used for all resonance pairs except the pair closest to the half-resonance of the transducer. For that pair the negative sign is used.

In the next section we compare the error in sample velocity using equation (A-9) to that obtained using the correction formulas derived by Bolef and Menes and by Ringermacher et. al. The "1 + δ" formula of Bolef and Menes[51] is written as

$$V_s \simeq 2\ell_s \Delta f_s^m \, (1 + \delta) \tag{A-10}$$

and is often used when δ is very small. Later, Ringermacher et. al.[34] derived an equation for V_s having improved accuracy and an extended useful range. Their formula is given by

$$V_s \simeq 2\ell_s \Delta f_c^m \left[1 + \delta \left(\frac{\pi D \Delta f_c^m}{f_c} \right) + \frac{\pi \delta f_t^2}{\Delta f_c^m} \, (DT^2 + T)^{-1} \right] \tag{A-11}$$

where

$$D = \frac{\cos \pi \, (f_c^m / f_t) \, \cos \pi \, \left[(f_c^m + \Delta f_c^m)/f_t \right]}{\sin \pi \, (\Delta f_c^m / f_t)} \tag{A-12}$$

and

$$T = \tan \pi \, (f_c^m / f_t) \, . \tag{A-13}$$

2. Computer simulated experiments

A. Two resonator experiments

In order to determine the accuracy of the approximate values of V_s from equation (A-9), the resonance frequencies of the exact two-resonator case were found by numerically solving equation (A-2) for an assigned value of V_s. All parameters in the equation were given values corresponding to a typical ultrasonic experiment. The sample was given values near those of aluminum 6.5×10^5 cm/sec for the sound velocity of 2.5 cm for the thickness, and 2.75 g/cm^3 for the density. The transducer was assigned values corresponding to lead zirconate titanate (PZT): 4.5×10^5 cm/sec for the sound velocity, 0.1 cm for the thickness (corresponding to a resonance frequency of 2.25 MHz), and 7.50 g/cm^3 for density. The percent error in the value of V_s obtained from equation (A-9) was calculated with respect to the assigned value of V_s and plotted as a function of the dimensionless parameter δ in figure 13. Also plotted in figure 13 are the percent errors using the approximations of equation (A-10), equation (A-11), and the uncorrected formula $V_s = 2\ell_s \Delta f_c^m$. The mechanical resonances used for these plots were the sixth and seventh resonance pair on the high-frequency side of the transducer resonance. As indicated in figure 13, the present approximation V_s generates an error which is smaller than the error in the other approximation formulas for each value of δ except for the largest value of δ shown (0.6).

The error in each of the formulas is strongly dependent on the choice of resonance pairs. In figure 14, the percent error in the present formula is plotted as a function of δ for a choice of

Figure 13.- Percent error in the value of the velocity of sound V_s, as a function of δ for various correction formulas in one transducer reflection case.

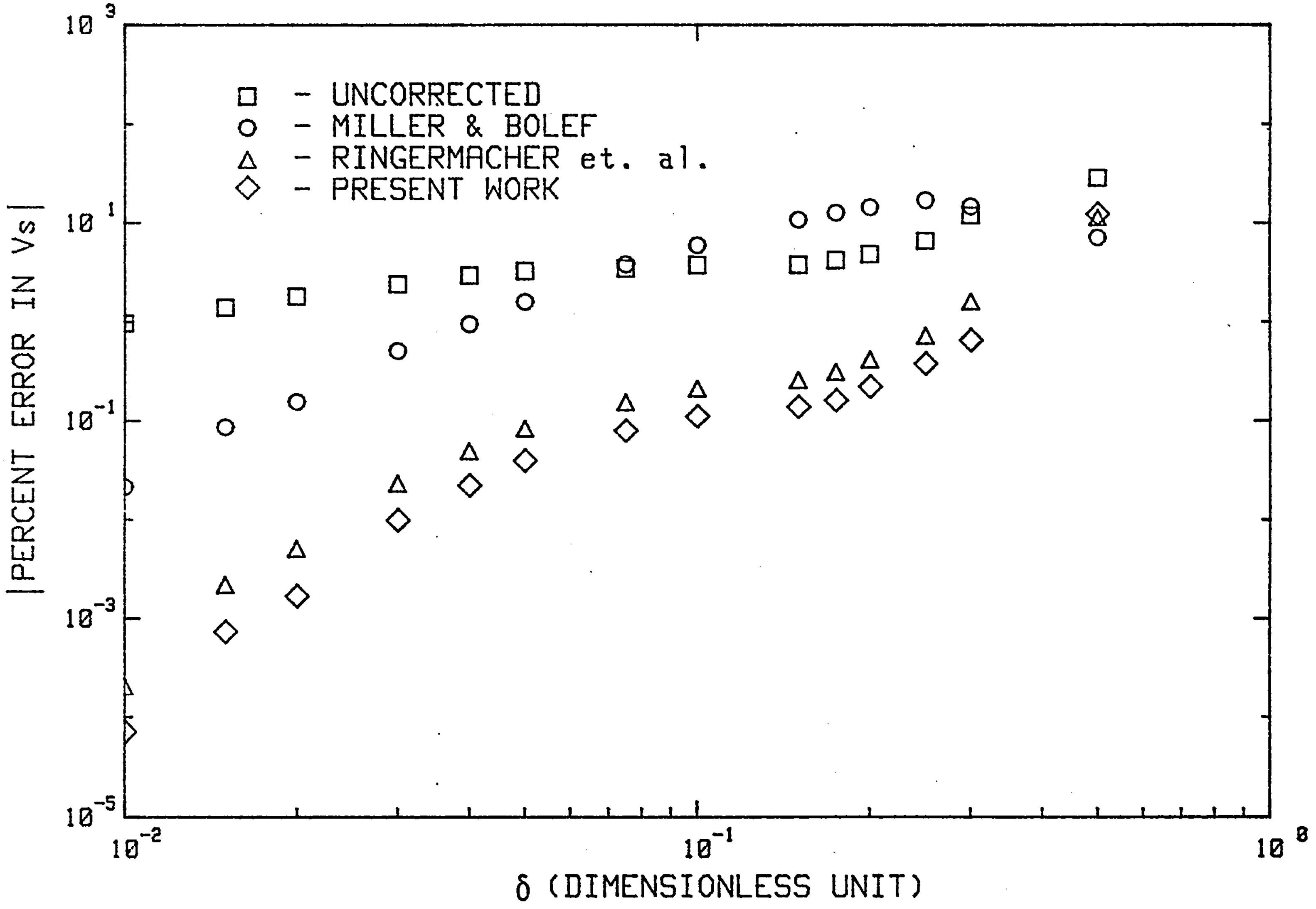

□ - UNCORRECTED
○ - MILLER & BOLEF
△ - RINGERMACHER et. al.
◇ - PRESENT WORK
|PERCENT ERROR IN Vs|
10^3
10^1
10^{-1}
10^{-3}
10^{-5}
10^{-2}
10^{-1}
10^0
δ (DIMENSIONLESS UNIT)

Figure 14.- Percent error in V_s as a function of δ for several pairs of mechanical resonances.

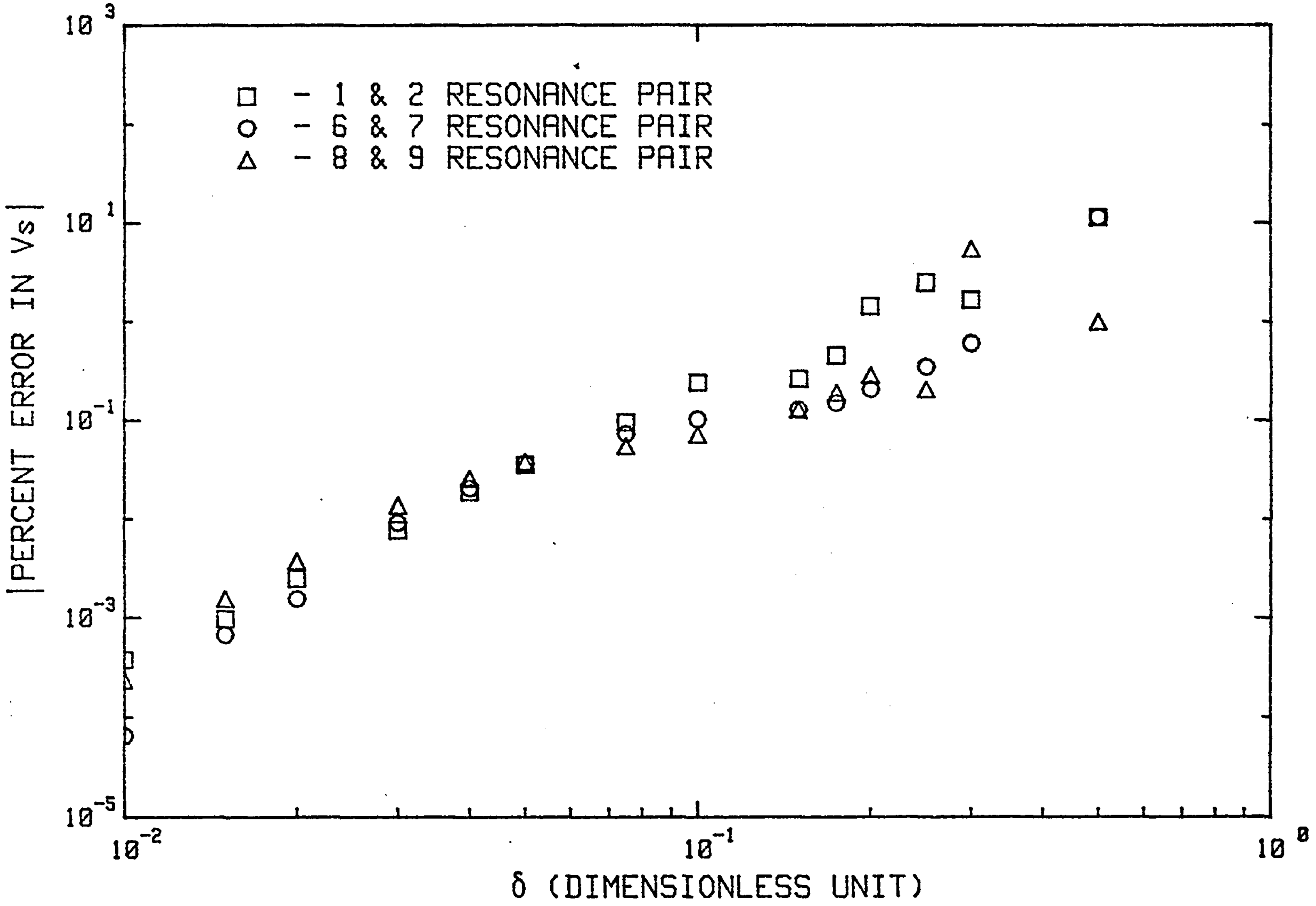
□ - 1 & 2 RESONANCE PAIR
○ - 6 & 7 RESONANCE PAIR
△ - 8 & 9 RESONANCE PAIR
|PERCENT ERROR IN Vs|
10^{3}
10^{1}
10^{-1}
10^{-3}
10^{-5}
10^{-2}
10^{-1}
10^{0}
δ (DIMENSIONLESS UNIT)

several resonance pairs. All resonance pairs used in figure 14 are on the high-frequency side of the transducer resonance frequency. Although a correlation between minimum percent error and a particular resonance pair is not apparent from figure 14, we see that the smaller values of δ typically result in less error for a particular choice of resonance pair.

Figure 15 shows plots of the percent errors in the four approximation formulas as a function of frequency $\delta = 0.109$. We see that the present approximation formula has the smallest error at each frequency point shown except the point nearest the resonance frequency of the transducer (2.25 MHz). There, the present approximation and the formula of Ringermacher et. al. are roughly equal in accuracy. Note that the minimum error for $\delta = 0.109$ is of the order of a few parts in 10^4.

Figure 15.- Results of computer simulated experiments comparing percent error in V_s as a function of frequency for 2.25 MHz PZT transducer bonded to an aluminum sample ($\delta = 0.109$).

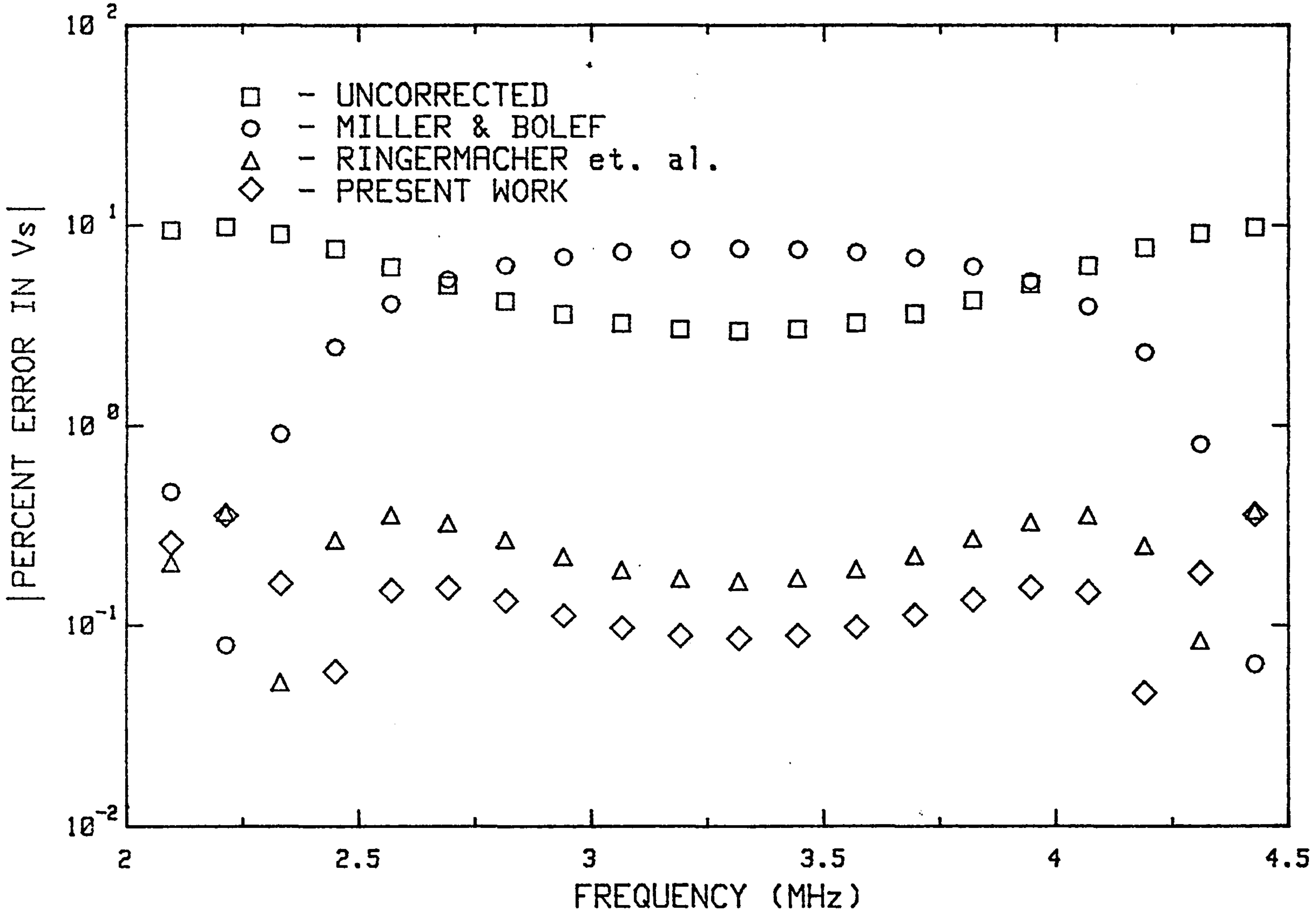

□ - UNCORRECTED
○ - MILLER & BOLEF
△ - RINGERMACHER et. al.
◇ - PRESENT WORK
|PERCENT ERROR IN Vs|
10 2
10 1
10 0
10-1
10-2
2
2.5
3
3.5
4
4.5
FREQUENCY (MHz)

B. Bond effects

We now consider the effect of the bond which couples the transducer to the sample surface. Bond effects on standing-wave measurements in solids have generally been neglected in the literature because the thin bond was thought to contribute negligibly to the measurements. We have examined the effect of the bond on the measurements of V_s by numerically solving equation (A-1) for mechanical resonance frequencies f^m_{tbs} of the transducer-bond-sample resonator and equation (A-2) for resonance frequencies f^m_{ts} of the transducer-sample resonator. Identical parameters for the transducer (PZT) with 2.25 MHz resonance frequency) and sample (aluminum) were used in equations (A-1) and (A-2). The frequency differences between adjacent mechanical resonance is Δf^m_{tbs} for the transducer-bond-sample resonator, Δf^m_{ts} for the transducer-sample resonator, and Δf^m_s for the isolated sample. The error in V_s was calculated from $(\Delta f^m_{tbs} - \Delta f^m_{ts})/\Delta f^m_s$ at each sample resonance frequency f^m_s between 0 and 5 MHz.

Plots of the percent error as a function of frequency for bond thicknesses of 1, 5, and 10 micrometers are shown in figure 16. Each point in the figure is at a resonance frequency of the sample. The curve is periodic with a period corresponding to the transducer resonance frequency. At multiples of the transducer resonance frequency the curves simultaneously pass through zero and each curve again passes through zero at nonperiodic points between the multiples. An important feature of all the curves in that the error increases as the frequency increases. The error also increases with increasing bond thickness and approaches a magnitude of approximately 0.6% at the higher frequencies.

Figure 16.- Plot of percent error for various bond thickness in one transducer case.

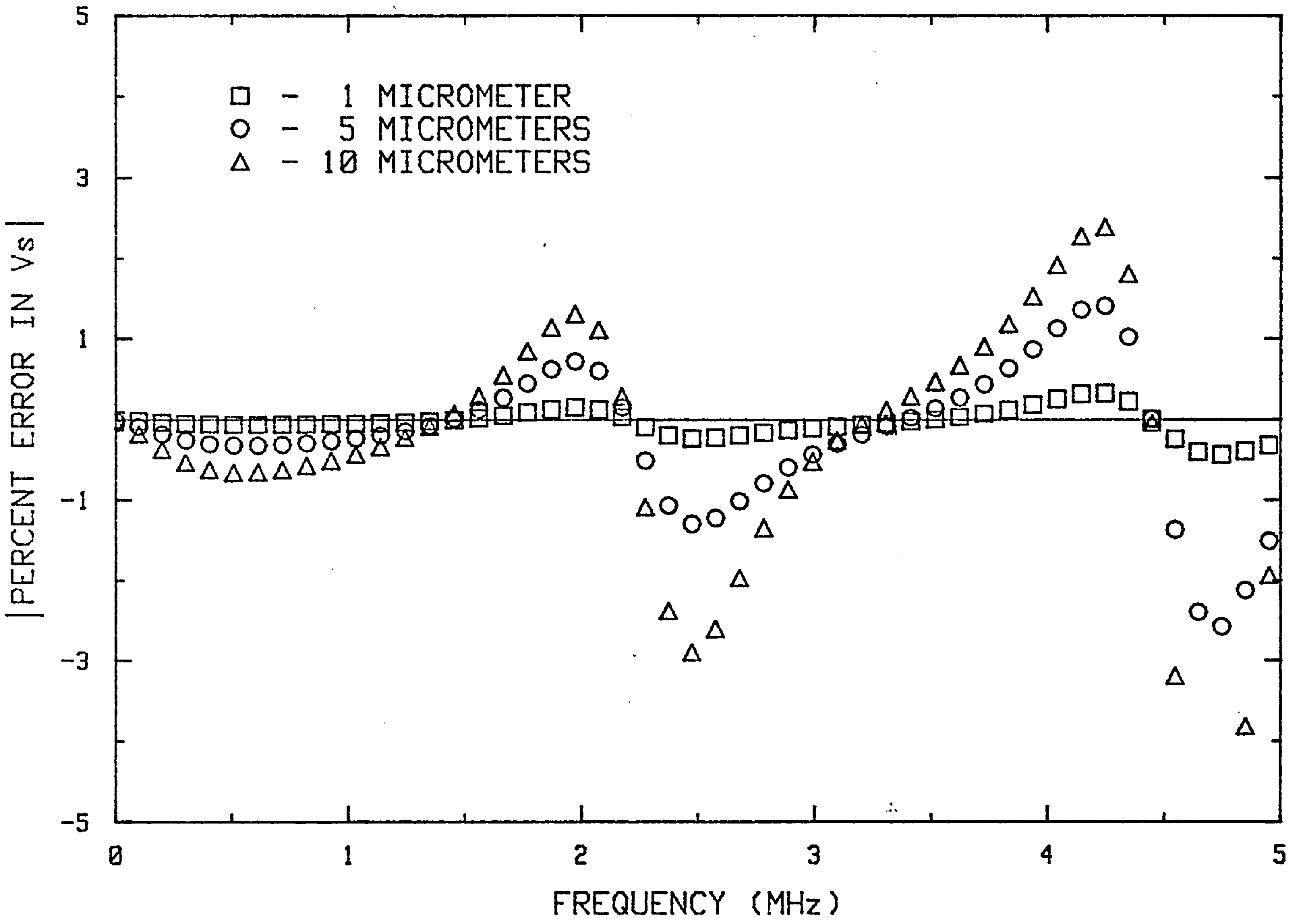
□ – 1 MICROMETER
○ – 5 MICROMETERS
△ – 10 MICROMETERS
|PERCENT ERROR IN Vs|
5
3
1
-1
-3
-5
0
1
2
3
4
5
FREQUENCY (MHz)

We conclude from equation (A-5) that the error due to the bond can in some cases be larger than the error in the two-resonator approximation formulas for V_s. Further, in order to minimize the contribution of the bond to the measurement error the bonds must be thin and the compound resonator resonance frequencies must be chosen as near as possible to the transducer resonance frequency.

3. Laboratory experiments

In order to test the above computer models, laboratory measurements were made on a 2.517 cm thick polycrystalline aluminum sample using the sampled continuous wave[21] (tone-burst spectroscopy) technique. Measurements were initially made with a 1.06 cm-diameter PZT transducer bonded to the aluminum sample with castor oil. To minimize bond effects, the first and second mechanical resonances on the high-frequency side of the transducer resonance frequency (2.065 MHz) were used. The value of V_s obtained from equation (A-9) were calculated to be 6.375×10^5 cm/sec.

An independent measurement of the sample velocity was obtained by replacing the single bonded PZT transducer with capacitive transmitting and receiving transducers. Since the capacitive transducers are non-contacting, the sample ends vibrated with effectively free-free boundary conditions and no transducer on bond corrections were required. Hence, the problem reduced to that of a simple standing-wave measurement on a single resonator - the sample.

The values of V_s obtained with the capacitive transducers is taken as the reference value for these experiments and was found to be 6.363×10^5 cm/sec. This value is 0.189% lower than the value obtained with the bonded PZT transducer using equation (A-9). The δ value for the bonded transducer measurements was calculated to be 0.115.

According to figure 14, the error in equation (A-9) for $\delta = 0.115$ is estimated to be +0.25% when the first and second resonance pair is used. The plus sign means that the bonded transducer measurement gives a value of V_s which is greater than the reference capacitive transducer measurement. The sign of the error and its significance was determined from an examination of the computer data which generated the point in the plot of figure 14. The magnitude and sign of the error is consistent with the error actually realized between the bonded transducer measurements and the capacitive transducer measurements.

The contribution of the bond to the contacting PZT transducer measurement error was minimized by selecting the compound resonator resonance pair nearest the resonance frequency of the transducer (f_t = 2.065 MHz) and by wringing the transducer onto the sample surface to minimize the bond thickness. The bond thickness was estimated to be 3-5 micrometers which according to figure 16 produces an error in the measurements of approximately -0.09%. The negative sign means that the effect of the bond is to yield a measurement of V_s with the contacting PZT transducer which is less than the reference value obtained with the capacitive transducers. Combining the -0.09% bond error with the +0.25% error in equation (A-9), we obtain a resulting theoretical error of +0.16%. This theoretical error is consistent with the +0.189% error measured experimentally.

For the particular choice of parameters used in experiments, the contribution of the bond to the measurement error is small compared to the error in the two-resonator expression for V_s (equation (A-9)). It is clear from figure 16, however, that a thick bond and a poor choice of resonance pair would have produced an error from the bond much larger than that from equation (A-9).

4. Conclusion

We have developed a more accurate formula for the explicit calculation of the sample velocity from standing wave measurements of the compound resonator. The limitations of the equation have been explored using computer models of typical experimental conditions. The accuracy of the formula increases with decreasing values of δ and depends on the choice of the resonance pair. Laboratory measurements of the sample velocity using a PZT transducer bonded to a solid were compared to measurements of the velocity using noncontacting capacitive transducers and were found to be consistent with predictions of the computer models using the present formula.

For a solid thickness of the order of a few centimeters, values of δ approaching 10^{-3} are practiably possible for frequencies of the order of 10 MHz or above. Such values of δ yield theoretical accuracies of parts in 10^{7} when the present formula is used. However, these accuracies are severely limited by one's ability to minimize the error from the bond. The present computer model of the bond error suggests that the theoretical limit can be approached only when the bond thickness is minimized and when the resonance pair nearest the transducer resonance frequency is chosen for the measurements. For liquid samples, bond considerations are not necessary and the theoretical limits of accuracy are more easily approached.

The correction formula for standing wave phase velocity measurements for the two transducer through transmission method is obtained using the same approach as in the one transducer reflection case. The derivation of the improved correction formula along with the computer and laboratory verification are given in detail in reference 37.

REFERENCES

1. R. N. Thurston and K. Brugger, Phys. Rev. 133, A1604 (1964).
2. D. C. Wallace, Phys. Rev. 162, 776 (1967).
3. J. H. Cantrell, Jr., Phys. Rev. B21, 4191 (1980).
4. J. M. Ziman, "Principles of the Theory of Solids," (Cambridge University Press, 1972).
5. C. Kittel, "Introduction to Solid State Physics," (John Wiley and Sons, Inc., New York, 1971).
6. K. Brugger and T. C. Fritz, Phys. Rev. 157, 524 (1967).
7. D. C. Wallace, in "Solid State Physics," Vol. 25, edited by H. Ehrenrick, F. Seitz and D. Turnbull (Academic Press, New York, 1970).
8. J. H. Cantrell, Jr., Proceedings of ASTM Symposium on Ultrasonic Measurements of Stress, April 1981. Accepted for publication in J. Testing and Evaluation.
9. E. J. Chern, J. S. Heyman, and J. H. Cantrell, Jr., Proceedings of 1981 IEEE Ultrasonics Symposium, October 1981.
10. J. H. Cantrell, Jr. and J. S. Heyman, J. Acoust. Am. 67, 1623 (1980).
11. J. S. Heyman, NASA patent disclosure LAR 12772-1 (1980).
12. A. Haug, "Theoretical Solid State Physics," Vol. I, edited by D. Ter Haar (Pergamon Press, Oxford, 1972).
13. M. W. Zemansky, "Heat and Thermodynamics," (McGraw-Hill Book Company, New York, 1968).
14. F. Reif, "Fundamentals of Statistical and Thermal Physics," (McGraw-Hill Book Company, New York, 1965).
15. E. A. Stern, Phys. Rev. 111, 786 (1958).
16. F. D. Murnaghan, "Finite Deformation of an Elastic Solid," (John Wiley and Sons, Inc., New York, 1951).

17. W. Voigt, "Lehrbuck de Kristall Physik," (Tribner, Berlin, 1928).

18. D. S. Hughes and J. L. Kelly, Phys. Rev. 92, 1145 (1953).

19. R. E. Green, Jr., "Treatise on Material Science and Technology," Vol. III, (Academic Press, New York, 1973).

20. J. S. Heyman and E. J. Chern, Proceedings of ASTM Symposium on Ultrasonic Measurements of Stress, April 1981, Accepted for publication in J. Testing and Evaluation.

21. D. I. Bolef and J. G. Miller, in "Physical Acoustics," Vol. VIII, edited by W. P. Mason and R. N. Thruston, (Academic Press, New York, 1971).

22. M. A. Breazeale, J. H. Cantrell, Jr., and J. S. Heyman, "Methods of Experimental Physics," Vol. XIV, edited by P. D. Edmonds (Academic Press, New York, 1981).

23. K. Brugger, Phys. Rev. 137, A1826 (1965).

24. E. Grüneisen, Hand. Phys., 10, 1 (1926).

25. Y. Hiki, J. F. Thomas, Jr. and A. V. Granato, Phys. Rev. 155, 764 (1967).

26. J. A. Garber and A. V. Granato, Phys. Rev. B11, 3990 (1975).

27. K. Salama and C. R. Ko, J. Appl. Phys. 51, 6202 (1980).

28. W. P. Mason, "Physical Acoustics and the Properties of Solids," (D. Van Nostrand Company, New York, 1958).

29. D. S. Hughes, W. L. Pondrom and R. L. Mims, Phys. Rev. 75, 1552 (1949).

30. R. T. Beyer and S. V. Letcher, "Physical Ultrasonics," (Academic Press, New York, 1969).

31. P. H. Rogers and A. L. Van Buren, J. Acoust. Soc. Am. 55, 724, (1974).

32. E. P. Papadakis, J. Acoust. Soc. Am. 42 1045, (1967).

33. H. J. McSkimin, J. Acoust. Soc. Am. 33, 12 (1961).

34. H. I. Ringermacher, W. E. Moerner and J. G. Miller, J. Appl. Phys. 45, 549 (1974).

35. H. I. Ringermacher, W. E. Moerner and J. G. Miller, Proceedings of 1974 IEEE Ultrasonics Symposium, IEEE Cat. No. 74CH0896-ISU, 555 (1974).

36. E. J. Chern, J. H. Cantrell, Jr., and J. S. Heyman, J. Appl. Phys. 52, 3200 (1981).

37. E. J. Chern, J. H. Cantrell, Jr., J. S. Heyman, and W. P. Winfree, Proceedings of 1980 IEEE Ultrasonics Symposium, IEEE Cat. No. 80CH1602-2, 946 (1980).

38. J. H. Cantrell, Jr. and M. A. Breazeale, J. Acoust. Soc. Am. 61 433 (1977).

39. M. S. Conradi (private communication).

40. R. J. Blume, Rev. Sci. Instrum. 34, 1400 (1963).

41. J. H. Cantrell, Jr. and E. J. Chern, Proceedings of 1981 IEEE Ultrasonics Symposium, October 1981.

42. K. Salama and C. K. Ling, J. Appl. Phys. 51, 1505 (1980).

43. R. F. S. Hearmon, Adv. Phys. 5, 323 (1956).

44. D. M. Egle and D. E. Bray, J. Acoust. Soc. Am. 60, 741 (1967).

45. R. T. Smith, R. Stern, and R. W. B. Stephens, J. Acoust. Soc. Am. 40, 1002 (1966).

46. E. H. Bogardus, J. Appl. Phys. 36, 2504 (1965).

47. G. K. White, Cryogenics, 4, 2 (1964).

48. S. Hunklinger and W. Arnold, in "Physical Acoustics," Vol. XII, edited by W. P. Mason and R. N. Thurston (Academic Press, New York, 1976).

49. G. K. White and J. A. Birch, Phys. Chem. Glasses, 6, 85 (1965).

50. J. H. Cantrell, Jr. and M. A. Breazeale, Phys. Rev. B17, 4864 (1978).

51. D. I. Bolef and M. Menes, J. Appl. Phys. 31, 1010 (1960).